university of groningen

THE EFFECT OF FAST CHARGER PLACEMENT ON TRAFFIC FLOW

By

SANDER BAKKER

A thesis submitted to
the University of Groningen
for the degree of
MASTER OF SCIENCE

California PATH
Department of EECS
University of California, Berkeley
March 2021

DEDICATION

This dissertation/thesis is dedicated to my family.

ACKNOWLEDGMENTS

The financial support that allowed me to move to California and write my thesis at one of the most prestigious universities in the world was provided by grants and scholarships from foundations, whose trust and generosity I am extremely grateful for. Without their support, I would not have been able to pursue this dream. The grants will be awarded to me upon successful completion of the research project and I declare no conflicting interests as a result of receiving these grants.

- Fundatie van Renswoude
- Groninger Universiteitsfonds
- Hendrik Muller Fonds
- Holland Scholarship
- Marco Polo Grant
- Van Eesteren-Fluck en Van Lohuizen Stichting

The effect of fast charger placement on traffic flow

by Sander Bakker, MSc.
University of Groningen
March 2021

ABSTRACT

First supervisor: Bayu Jayawardhana, PhD
Second supervisor: Ashish Cherukuri, PhD

Daily first supervisor: Murat Arcak, PhD
Daily second supervisor: Alex A. Kurzhanskiy, PhD

The market of electric vehicles is expected to grow as a result of governmental incentives to combat climate change. Previous research has established the need for electric vehicle charging stations to accommodate electric vehicle market growth. Other research looked into ways to optimise cost of construction and operation as a result of charging station placement and some consider the effects on the power grid. However, no study has considered the effect that placement of these charging stations, and in particular direct current fast chargers, has on traffic. This research makes use of an agent based model and OpenStreetMap to simulate and study the effect of charging trips as a result of fast charger placement. A case study from the city of Berkeley shows that for different placement policies, vehicles which update their route choice experience an increase in travel time close to the charger locations, i.e. on city blocks that connect to the intersection that provides access to the charger. Vehicles that do not update their route choice experience additional delays when merging onto the high capacity, arterial, roads along their shortest path to the fast chargers.

Table of Contents

List of Figures

List of Tables

1

Introduction

Electric vehicles (EVs), or plug-in electric vehicles (PEVs) [1], are defined as vehicles that are powered with a rechargeable on-board battery. EVs include both plug-in hybrid electric vehicles (PHEVs) and battery electric vehicles (BEVs). The total number of EVs, including BEVs and PHEVs, in 2021 was approximately 16.5 million: EV market shares increased by over 70% in Europe, doubled in the US and even tripled in China [2]. The Paris Declaration on Electro-Mobility and Climate Change has set a goal for 100 million electric cars across all market segments by 2030 [3]. In order to reach this goal, the market for EVs is to grow largely. There are however some barriers such as high purchasing cost, limited driving range, the lack of an appropriate charging infrastructure and consequently range anxiety [4–6], i.e. a combination of the preceding two barriers.

1.1 The market of electric vehicles

Note that the statement that charging stations (CSs) are not built to supply an increasing number of EVs, but EVs are sold due to the increased number of CSs [5, 7]; since the construction of CSs does not follow a market logic yet and is rather driven by subsidies, regulations [8] and neighborhood effects [9], i.e. people influencing one another at home or at work influencing new EV sales. This EV market exhibits indirect network effects due to interdependence between EV adoption, i.e. the demand side, and charging station investment, i.e. the supply side [8]. Subsidizing either side of this market, e.g. through EV purchasing incentives such as subsidies on the demand side, or through construction of EV charging infrastructure on the supply side. Governmental interference on the demand side is applied in countries in which EVs have significantly high market shares such as the Norway, the Netherlands [10], and California. In the latter (state), new incentive legislation on the sales of passenger vehicles requires all new passenger vehicles to be zero-emission by 2035 [11]. Construction of EV infrastructure also has a positive effect on EV sales [12, 13]. It was found however, that subsidizing charging infrastructure results in larger EV adoption compared

to EV purchasing incentives [8], which is in line with the previous statement. Adoption models resulted in a a 3% increase in EV purchases per capita for every additional CS per capita [13].

Due to barriers mentioned in the first paragraph, BEVs are currently not utilized to their full capacity. Range anxiety is the fear of depleting the battery and therefore lack sufficient range to complete a trip, leading to under-utilizing the available range and limit the distance travelled in a BEV, even when the BEV is capable of adequately completing the required journey. It is to be solved by making public charging broadly available, bringing many lower mileage drivers to near-100% utility while strongly increasing the travelled distance of high mileage drivers [14].

1.2 Electric vehicle charging

Three types of EV chargers exist, the division is based on their power ratings, an overview of which is provided in Table 1.1. Level 1 and 2 chargers use alternating current similar to residential electricity supply. Note that level 1 charging at 120 V is only available in the US [15], a single phase charger delivers 1.4 kW - 1.9 kW at maximum for currents ranging from 12 A to 24 A on 16 A and 20 A circuits respectively [16]. Yet, using a single phase charger in Europe, e.g. in the Netherlands, is likely to deliver 3.7 kW at maximum, since most residential sockets deliver at most 16 A at 230 V in 25 A circuits [17]. This is at most twice the amount of power delivered by level 1 charging in the US. However, in terms of power output, this is not the range of level 2 charging power, which typically supplies more the current, leading to power output ranging from 7 kW to 20 kW [18, 19]. Note that [20] sets the typical power of level 2 charging to 20 kW, this has been used in Table 1.1 and provides more distinct insight in the attainable capacity of different charging levels. Attainable in this sense refers to the power output offered by the CS given the supplied voltages and currents in that particular level.

Table 1.1 Charging power levels from [20].

Charger type	Typical use	Typical voltage	Typical power	Charging time
Level 1	AC residential	120 V	2 kW	4–11 h
Level 2	AC public	240 V	20 kW	1-4 h
Level 3	DC fast	400 V	100 kW	< 30 min

With level 1 and level 2 charging, CSs determine the amount of electricity that a car can take form the grid and the car does the charging, i.e. through conversion to direct current for supply to the car battery. Level 3, or direct current fast chargers (DCFCs) work differently, their voltage is much higher and the supply of direct current voids the constraints of onboard battery chargers. Due to

the high voltage and power output, Level 3 is therefore mainly intended for public and commercial facilities [19]. Market analyses and simulations in previous research have established that the prevalence of DC fast chargers in particular is an important factor for consumers' acceptance of EVs, driving their adoption [6].

1.2.1 Power grid implications

The electricity demand for charging EVs gives rise to additional loads on existing distribution systems ensuing energy losses in the system leading to decreased phase voltage [19]. DCFCs instigate voltage drops which are only to be dealt with by high capacity, or strong, buses near generation sources [21]. Explanation on how this part of the distribution network works has been provided in Section A.1. This section addresses two major impacts on the power grid, also referred to as the energy distribution system, provoked by DCFCs are summarized in the two key items:

1. grid load capacity;
2. power quality;
    (a) voltage discrepancies;
    (b) harmonic distortion.

Non-coordinated charging, i.e. random or erratic, hugely increases load on the power grid, especially during peak hours, reducing the capacity even more [22]. Peak hours occur typically between 4 p.m. and 9 p.m. [19, 23], when energy demands in all sectors coincide [24] and hence supply becomes scarce.

Aforementioned voltage drops and offsets, or discrepancies, are often caused by people simultaneously requesting high charging currents all at once, this typically occurs at the start of charging actions at DCFCs since those require high current at an instant [22]. Offsets in particular are caused by reactive components in power grids [25], often seen in electric devices. Hence, people driving home from work and charging their car using a DCFC, e.g. during peak hours, will amplify the effect of voltage deviations [19], especially affecting the distribution section of the power system [26, 27]. With a DCFC operating at its fast charging state, i.e. before battery state of charge (SOG) reaches 80%, the total harmonic distortion (THD) value in the peak hour is above 10% [19, 27], which might cause equipment to fail. Harmonic distortion is often caused by the conversion from alternating to direct current, in particular when using non-linear circuits like rectifiers used for power factor correction (PFC) [25, 28] in DCFC installations, i.e. correcting the phase displacement of current to match with voltage and subsequently reduce (magnetizing) power losses

[29]. THD implies that the (voltage) waveform has become distorted, this could lead to transient over-voltage [30] causing the transformer to malfunction and possibly heat up [31].

Distribution system overloads occur when power draw on a line exceeds rated limits of components. It is critical to manage loads, e.g. by means of voltage compensation in the distribution feeder during peak hour [19], and upgrade systems appropriately to prevent line and transformer overloading which could require costly upgrades [27, 32].

1.3 Placement of electric vehicle charging stations

Many researchers have looked into optimal placement of public EVCSs, in particular DCFCs, from different perspectives, these are subdivided in the following categories: charging stations operators, EV users and distribution network operators [33]. For most optimization problems in the three categories, monetary cost, e.g. of construction and exploitation [34, 35], is considered in the objective function. However, some research in the latter category considers power loss cost and voltage deviation cost in the objective function [36–40]. In [39] maximise profit, through penalising power losses due to their effects on network power quality and in [40] on maximizing flow-based EV charging load demand, since demand is not always expressed at the nodes and the mobility of EVs results in dynamic demand. The authors of [36] provide a clear method on EV load profile prediction. Through using copula functions, which relate marginal cumulative distribution functions [41], in this case of arrival time, departure time and travelled distance, to their joint distribution function, i.e. charging demand.

These studies however do not take into consideration the implications to the power grid as touched upon in Subsection 1.2.1 and the real world has proven that the grid often may not be capable of providing the required loads on the desired locations [7, 42].

2

Problem analysis

Even though a couple of researchers have established the effect of EVCS placement on adoption, as explained in Chapter 1, there are no studies on the effect that these stations exhibit on traffic (flow), to the best of the author's knowledge. EVCSs are different in nature than petrol, or gas, stations, in which the filling up and paying takes a couple of minutes and capacity is usually not an issue. EVCSs might have limited charging points, as the grid might not be able to cope with additional loads and charging typically takes up to half an hour (Table 1.1). Thus, these EVCSs might lead to, or induce, different traffic flows, due to their capacity and waiting time leading to queues, especially if more people, also without access to residential CSs, adopt to using EVs.

2.1 Problem statement

It is currently unclear if, and to which extent EVCSs affect traffic conditions, in particular road congestion. The placement of these stations might cause people with EVs to deviate from the routes they would originally drive in order to charge their vehicle.

The resulting traffic flows from charging actions will in this study be referred to as "induced demand". It has been established that charging of EVs, BEVs in particular, takes much longer than filling up internal combustion engine vehicles (ICEV) with petrol, or gasoline, which entails that the service rate of customers, per charger per unit of time, is generally smaller than a single petrol pump, present at filling stations. Additionally, CSs have less charging ports than filling stations have pumps. Therefore, it is expected that induced demand has an effect on traffic congestion.

3

System description

This chapter moves on to describe in greater detail the system that will be considered for treating the aforementioned problem. The following sections will elaborate on the elements of which the system comprises and a concluding section will summarise their interactions through the use of a block diagram.

3.1 The traffic network

The system of this research consists of a traffic network, obtained from OpenStreetMap (OSM) using the OSMnx Python package. The OSM traffic network, hereafter also referred to as (road) network, is best interpreted as a directed graph, $G(V,E)$ existing of $|V| = 1449$ vertices, or nodes which represent intersections (junctions), and $|E| = 4957$ edges, or links, represented as $l(u,v) \in E$ to indicate the node pairs it connects or l for short. The links represent roads in the network, these connect the nodes and are unidirectional, i.e. agents can move in one direction along the links. Consequently, two (adjacent) links are used to connect an equal set of two nodes to facilitate two-way traffic in the traffic network, e.g. $l(u,v) \in E$ and $l(v,u) \in E$. The network has been simplified using a built-in function from the OSMnx package, namely the `consolidate_intersections` function [43] with tolerance set to 0.0003. A graphical representation of the network is provided in Figure 3.1.

3.1.1 Node and link data

In order to use this OSM data in simulations, a data-frame is constructed for both the nodes and the edges in the traffic network. The node data-frame stores the latitude, longitude, OSM identification number (ID) and assigns a node ID to all rows in this data, i.e. the nodes V are enumerated from 0 to $|V|$ in the traffic network, e.g. if there are 3000 nodes in the model, node IDs range from 0 to 2999 as Python starts indexing with 0, this is done to allow for iterative calculations and since

Figure 3.1 Simplified OSM graph of Berkeley obtained using OSMnx, the graph has 1449 nodes and 4957 edges.

the OSM node IDs are less intuitive nor easy to work with, e.g. nodes which are separated by a couple of meters may have completely different length and starting numbers, see the examples in Section A.2.

The edge, or link, data-frame stores more attributes for each link as compared to the node data. Similarly to the node data, an ID is assigned to all links in the network. Each row stores the a link ID, starting model node ID of link, ending model node ID link, length, speed limit, number of lanes, the capacity in terms of vehicles per hour, free-flow link traversing time in seconds which is based on the speed limit and link length, starting OSM node ID, ending OSM node ID and the geometry, a line-string with the latitude and longitude data of all the nodes that the particular link connects.

3.2 Traffic network demand data

In addition to the OSM traffic network, this study uses real traffic network demand data downloaded from Replica a web service that provides data on the built environment of North America [44]. This data helps with simulating real-world road usage with the agent-based model (ABM). Previous studies with the ABM have made use of probability distributions for trip origin and destination locations [45]. Replica's demand data is provided in terms of origin-destination (OD) pairs in terms of latitudes and longitudes of block groups to indicate the starting and ending position of agents in the network. Additionally, this demand data exists of trip start time and end time, building use for both locations, which might be useful for extracting commute trips as an extension, and vehicle IDs of the trip-takers, or agents, allowing for traceability.

Figure 3.2 Heat-map of origin coordinates present the autumn 2021 data, the base scenario, from Replica. The coordinates of the heat-map centroids represent a cluster of origins located within 15 mm of the full-sized graph for readability purposes.

Figure 3.2 provides a graphical representation of the original Replica data of autumn 2021. It can be seen that many trips depart from Downtown Berkeley and close to the University of California

campus. In addition to the heat-map, a histogram that shows trip departure frequency for every 5 minute interval of the demand data is provided in Figure 3.3.

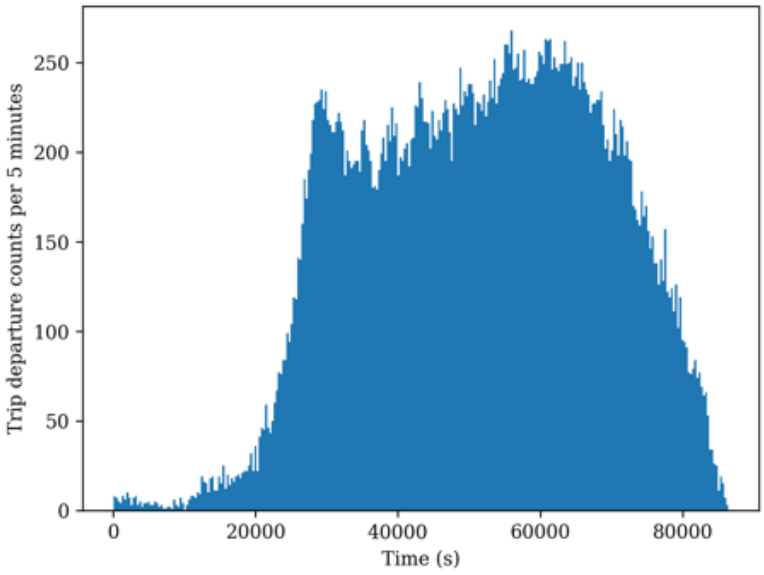

Figure 3.3 Histogram of trip departures for every 5 minute interval in the autumn 2021 demand data from Replica.

3.3 The agent-based model

All system elements from the previous sections conjoin as inputs to Bingyu Zhao's macroscopic agent-based traffic model (ABM) [45, 46]. The model receives as inputs the aforementioned network (Subsection 3.1.1) and the demand data (Section 3.2).

Agents enter the network on nodes at the trip starting times stored in the OD file, agents are not allowed to enter the network on links. Nodes store a particular pre-depart count, i.e. the number of agents which is to depart from the node, which allows for insights in where trips depart from and how many. The link data-frame stores several interesting properties along the basic properties such as the connecting, i.e. starting and ending, nodes, geometry, length, speed limit and the number of lanes. Additionally, capacity is calculated based on the link length and the number of lanes.

Now, in order for agents to manoeuvre through the network after entering the network in an efficient and realistic manner, a Dijkstra shortest path (sp) algorithm [47] is used to find the shortest

path to the destination using link traversing times as weights. The initial condition of link traversing time is the free-flow time along a particular link, i.e. traversing exactly at the speed limit along the entire link length. The traversing time of the link is updated every time, t, or iteration, based on the average travel time along the link of other agents of the past 60 seconds. The simulation outputs multiple files, among which the aforementioned node and link statistics. Especially the link statistics store particularly useful properties such as the run and queue vehicle count, i.e. the moving and stationary vehicles across a link, for each time, t. The latter two parameters provide useful insight in the link usage and logically depend on the link capacity.

The model exists of four classes, which hold dictionaries and functions to capture the behaviour of the model and store information each time-step: Node, Link, Agent and Simulation. The Node class stores the exact location of each node, along the links that connect to it and the vehicles which are to depart from the node at the current time-step. The Link class stores its location, available as well as incoming, outgoing and total storage capacity and the vehicles that pass through or currently are queued on the link. The Agent class stores origin, destination as well as departure time, keeps track of the current node or link that the agent occupies and does the routing part, i.e. finding the path through the network along connected nodes and links to get from the agent's origin to their destination. The Simulation class initialises the simulation by extracting the demand as well as the the connected graph and makes dictionaries for all nodes, links and agents which are to be updated across all other classes.

3.4 System

This chapter has reviewed the three key aspects of the system in this study. The preceding sections are connected through the use of a block diagram to provide a visual overview and intuition of how all elements, its inputs and outputs relate in Figure 3.4. In the figure, the arrows within the ABM have been labelled using a letter due to a lack of space. Arrow (a) represents node, link and OD demand data-frames and the end time of the simulation. This data serves as input to functions defined in `queue_model.py`. Arrow (b) represents network data and trip information such as current node in the simulation and trip destination node. The sp algorithm finds the shortest path and it outputs arrow (c), representing the (shortest) paths, consisting of a list of nodes for all agents present in the OD data-frame. Arrow (d) represents simulation results from the queue model, among which are the raw node and link statistics. The `simulation_queue.py` code converts this raw data into intuitive csv files, storing vehicle queue counts among others, as explained in Section 3.3.

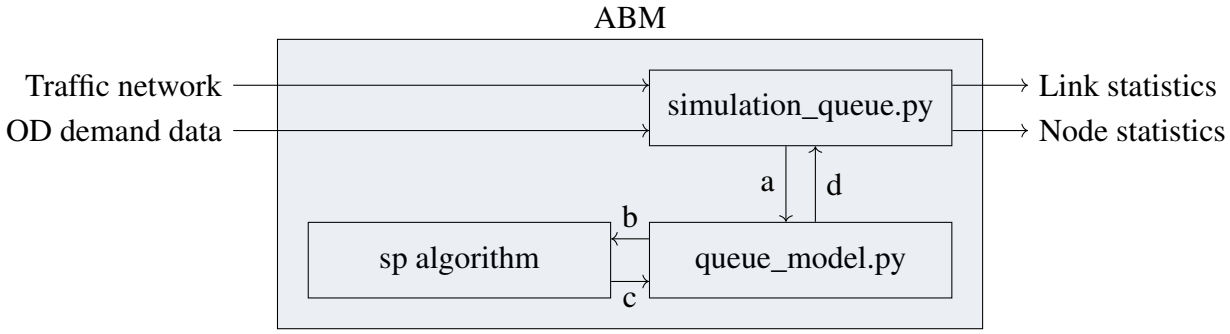

Figure 3.4 Graphical overview of the system of this research. All system elements within the blue box are part of the ABM. Function calls have been depicted by arrows and the blocks represent files containing code, their execution results in outputs, i.e. arrows starting from the block, the value of which depend on the input, i.e. arrows ending in the block.

4

Research contribution

This chapter provides an overview of the goal to which this research answers, along with the guiding research questions to reach that goal. Moreover, a section is devoted to how findings of this research will be presented to the reader.

4.1 Research goal

The goal of this research project is to visualise the effect of "induced demand" on road congestion indicators such as road density or link traversing time to identify new traffic bottlenecks prior to EVCS placement in the public infrastructure, and the degree to which these indicators relate to placement on different locations throughout the area of study. This goal is achieved through using Bingyu Zhao's macroscopic ABM [45, 46] for simulations of charging traffic flows resulting from EVCS placement, i.e. "induced demand", for EVCS placed on different locations, and potentially for different levels of EV penetration, and comparing these results to current traffic conditions in the city of Berkeley.

4.2 Research questions

The main research question is: *what is the effect of the "induced demand", resulting from EVCSs placement, on traffic flow?* Now, in order to answer to the main research question, several sub-questions are listed below. Answers to these questions will shape the structure of this thesis and ultimately lead to answering to the research goal. The sub questions read:

1. In what way can Zhao's ABM contribute to studying the effect of EVCS on traffic?
2. What is the charging demand for charging stations at different locations?
3. How is charging demand translated into trips in the simulation?

4. What is the ratio between EV drivers having access to residential charging and EV drivers who rely on public DCFC infrastructure?
5. What are potential locations for EVCS placement?
6. How do different placement locations influence traffic?
7. To what extent do simulations aid in identifying new traffic bottlenecks after EVCS placement?

4.3 Operationalistaion

Among the sub questions are also questions that simply require the availability of data, among which are the first, second, fourth and fifth. This data will prove useful in ABM simulations, and prove useful for defining and editing system inputs such as the OD demand data.

However, with the intention of using the ABM for simulations with historical, real world, data, its performance is to be validated. This can be done by comparing trip duration, or arrival times, from the simulation and the data. When the model proves to simulate real world behaviour and produce results of substantial similarity, different placement policies are researched to investigate the effect that the induced traffic demand from EVCS placement has on the aforementioned traffic conditions. This would aid answering to the first and seventh sub question.

The following chapter will be devoted to answering to the third and fifth research sub questions. Procedures and methods used in this study along with arguments to support those considerations will be put forward. Modelling of charging trips will be subsequent to the following chapter and the focus will be on answering the sixth sub question.

4.3.1 Deliverable

In order to answer to the research goal, this research is to deliver a visual overview of traffic conditions, in particular new bottlenecks, that result from EVCS placement and charging trips. Traffic conditions, in particular road congestion could be expressed by the number of queued vehicles on a particular network link. These queues could either be visualised as colour-scale projections on the actual map to intuitively show road link usage and (additional) travel time.

5

Methods

In order to perform simulations jointly with the OSM traffic network and the demand data, modifications have to be made to both. This chapter will cover methodological considerations on how the ABM is validated for use in this research as well as considerations for treatments to the following problems: simplification of the traffic network, the introduction of CSs in the network model, the misalignment between the aforementioned data sources.

5.1 Model validation

Before using the model for the aforementioned implementation, the model will be validated for use within the system of this research in accordance with the first research question from Section 4.2. As explained Section 3.3, the ABM deploys agents on an origin node at the corresponding trip start time and iterates over time whilst moving the agent through the network to its destination along their shortest path. This entails that the arrival time can be extracted from the simulation, by storing the time-step at which an agent arrives at the destination node. Additionally, the OD demand data extracted from Replica contains trip arrival times. Hence, a comparison between the two is made for all agents to evaluate the (relative) change in trip duration, i.e. dividing the difference in trip duration by the actual trip duration, to validate the performance of the ABM.

In order to answer to the first research sub-question, this section is devoted to answering how the ABM can be of aid in this research. The performance of simulating real world travelling behaviour is tested with data real world from Berkeley. In particular, a data-set from Replica is extracted using the following filters:

1. Only trips from trip takers having home location in one of the 13 zip codes that make up the area of study, as displayed in Section 3.1, have been taken into consideration. The zip codes considered have been listed in Section A.3.

2. The primary travel mode of trips is chosen as private auto.

3. The extracted trips are from a typical Thursday in the autumn of 2021, which is the most recent trip data (as of December 2022). Replica allows users to either select a typical Thursday and typical Saturday, representing a weekdays and weekends respectively.

Only including private auto trips removes all trips which will not be able to maintain the speed limit, e.g. people riding bicycles and walking, and prevents double counting since auto-passenger trips are excluded. Additionally, this filter excludes public transit, which makes up a small percentage of the total trips, namely 5.12% compared to the 46.5% of private auto. The OD data, after application of the previous filters contains 317,000 trips out of in total 681,000.

Additionally, trips that originate from and arrive the same node are considered redundant and are removed from the data, as there is no information available on where the trips go in terms of intermediate nodes. Moreover, trips that either start or finish more than a specified distance, e.g. 500 meters, outside of the network are disregarded. Origins and destinations of those trips would be assigned to the bordering network nodes causing unrealistic congestion around the network borders and unrepresentative arrival times, as the trips may arrive earlier at the bordering nodes than at their destination, which might be 60 miles, or 100 kilometers, outside of the network. The remaining OD data, after filtering based on the foregoing conditions, contains 176,000 trips.

5.1.1 Model calibration

The ABM is not designed to come up with a random trip between two nodes, but provide the shortest path instead. Furthermore, there may be many trips starting and ending outside but going through the network, hereafter also referred to as background traffic, that heavily influence the available road capacities and speeds, e.g. cut-through vehicles on the adjacent lane to the off-ramp that impede the through movement traffic, decreasing the road capacity as a consequence [48]. Additionally, the model does not include intersection modelling, e.g. agents losing time due to the order in which they are to cross an intersection. Moreover, people might not be rational in determining route and lastly, trip takers may go for intermediate stops on their trip causing them to reroute from the shortest path, e.g. going out for dinner and picking someone up during the trip to the restaurant. To conclude, this paragraph has analysed the potential causes of the discrepancy between simulation and actual arrival times.

Moving on now to consider that simulations 24 hours may take a long time to complete, a smaller part of the day, e.g. the evening rush hour, can be used to analyse the sensitivity of network link parameters. The parameters of interest are link capacity and link speed. These parameters,

in particular the link capacity can be used to mimic the presence of background traffic during the simulations. The goal of calibration is logically to adjust the parameters in such a way that simulation arrival time more accurately approximates actual arrival time.

5.2 Network model

As briefly touched upon in Section 3.1, this study uses a simplified OSM network: it is a direct input to the ABM as show in Figure 3.4. Additionally, intersection consolidation is used with a tolerance set to 0.0003. This tolerance represents a radius for each node in the network: when other nodes lie within each other's radii, they will be merged and their centroid will become the consolidated, or new, network node as can be seen in Figure 5.1b. The reason for this simplification is that OSM nodes are most often used to define the shape or "path" of a road, or way [49]. This entails that multiple OSM nodes may constitute roads or intersections and hence, add unnecessary complexity to the model. Furthermore, the ABM assigns a particular vehicle length to each vehicle of 8 meters, taking into account vehicle length as well as safe distance from other vehicles, therefore the vehicles might not be able to travel over these links and if they do it might yield misleading or unrealistic link parameter characteristics to the ones listed in Section 5.1. Figure 5.1a displays the raw OSM network obtained using the OSMnx package, it should be noted that intersections constitute of 4 separate OSM nodes, e.g. the close parallel lines in the middle of the image from left to right with an upward slope represent University Avenue.

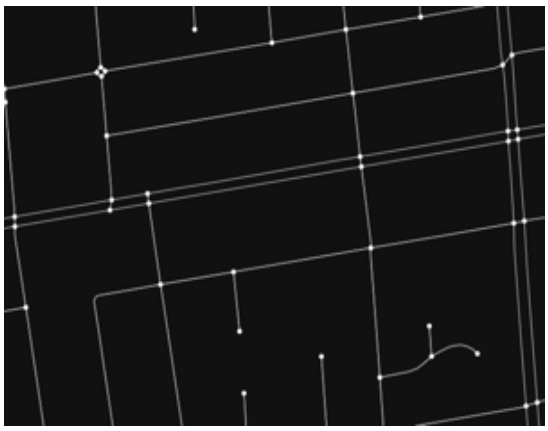

(a) Original, or raw, OSM network existing of multiple nodes per intersection.

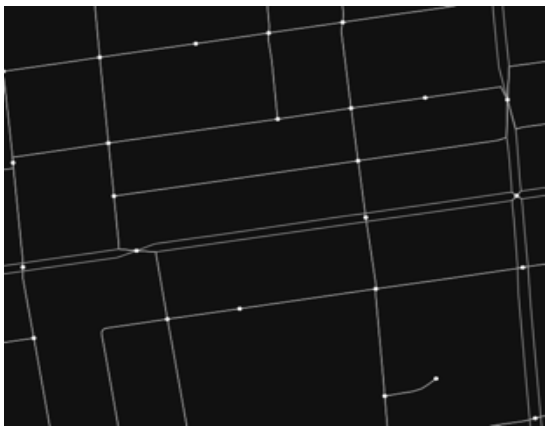

(b) Simplified OSM network with consolidated intersections.

Figure 5.1 Comparison between the original and simplified OSM network of a block group in Central Berkeley.

Provided that the consolidated, or new, nodes are not on the exact same position as the OSM

network nodes, they will be assigned an arbitrary OSM node ID, which happens to be in line with the node IDs which are assigned in range, i.e. in ascending order starting at 0. However, keeping this additional column of OSM node ID brings some advantages that will prove useful to answering the third research sub-question as well, elaboration on which will be provided in the following paragraphs. Additionally, some nodes might not be consolidated and hence keep their original OSM node ID, which would complicate iterative data processing. Therefore, both the node ID and OSM ID will be stored in the node data-frame.

5.3 Alignment of demand data and network model

Assigning the origin-destination (OD) data from Replica to the OSM network brings some difficulties: the latitude longitude pairs of the demand data do not exactly align with the nodes present in the OSM network, as data from Replica corresponds to centroids of block groups instead of intersections. As mentioned before, it is necessary to assign trips to network nodes: the system, and in particular the `simulation_queue.py` code is only able to receive demand data starting from and ending in the network nodes from its other input, namely the node data as can be seen in Figure 3.4. Two ways to treat this problem are considered:

1. Assigning the demand data to the closest node in the network (Figure 5.2b), and therewith assuming that people use the geographically closest entry point into the road network. This distance could either be calculated using either a Haversine function or using Pythagorean theorem through Cartesian coordinates for simplicity.

2. Extending the OSM network through adding nodes and edges to model this behaviour. Including (smaller) streets, e.g. residential streets, from which drivers might originate and additional nodes which represent the exact road entry points for all houses (Figure 5.2a).

Even though the first method might allow for more realistically model the traffic dynamics also in residential streets, there are multiple arguments for using the second method. Firstly, considering that smaller residential streets often lead to nodes that are in the OSM road network, i.e. entry points to the higher capacity roads, within a couple of blocks. Secondly, the goal of this agent-based macroscopic traffic simulation model is to decrease computational cost, when compared to microscopic traffic simulation software like Sumo, often used in many previous transportation studies [50]. To clarify, macroscopic models capture traffic dynamics in lesser detail, but are faster and easier to apply and calibrate than microscopic models [45]. However, the goal of this research is to identify the influence of EVCS placement on traffic and to visualise the potential new bottlenecks caused by this induced demand. Lastly, the goal of this study is not to focus on residential

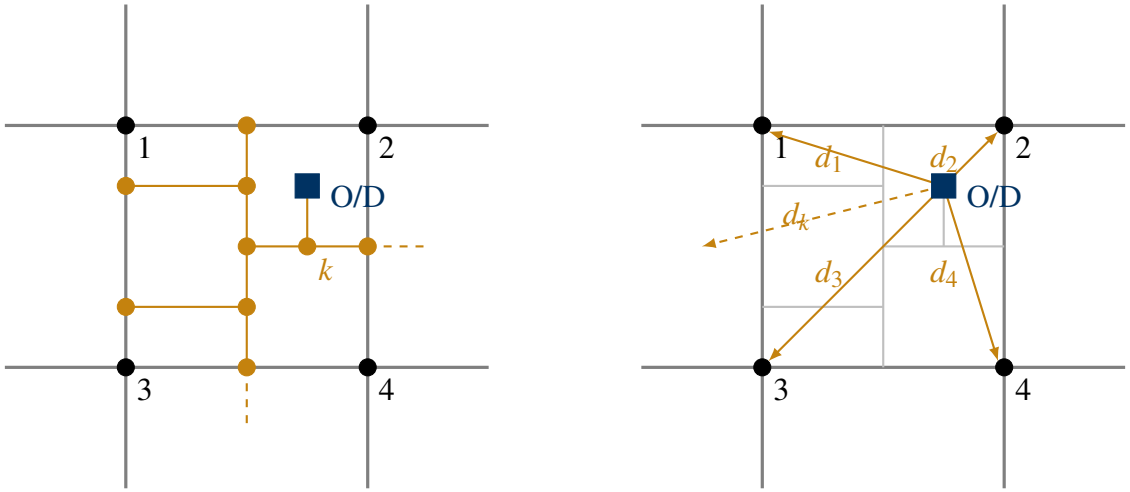

(a) Adding nodes and edges, depicted in brown, to the existing OSM network to more closely match OD data locations.

(b) Assigning demand data to closest node of the OSM network, this distance is depicted with brown arrows.

Figure 5.2 A simplified graphical overview of treatments to misalignment between OD demand data, depicted in dark blue, and the OSM network nodes $k \in V$, depicted in black. The light gray edges in Figure 5.2b are not part of the OSM network.

streets in great detail, which is in line with the previously stated on reducing complexity and computational cost.

In conclusion, the second listed treatment is considered more suitable over the first and will hence be used to treat misalignment of OD data and OSM network for this research project. In terms of calculating the shortest distance from OD data to network nodes, two methods have been proposed in the second item above the previous paragraph. Now, calculating this distance using Pythagorean theorem, i.e. orthogonal distances, might lead to "errors" [51] when approaching meridians [52], when compared to using a Haversine function, most often used when calculating distance between two points on a ball, like the earth [53].

5.4 Addition of charging stations to network model

In order to facilitate EV charging in the ABM simulation with CSs, to which they can navigate during the simulation to charge, these CSs are to be added to the OSM network model. Two approaches for introducing CSs are considered:

1. Extending the OSM network through adding a dummy node, representing the CS with Figure 5.3a as its `OSM_node_id` similar to the previously listed method, and an dummy link, representing an entrance and exit road, as depicted in Figure 5.3b.

2. Converting a network node into a charging station (access) node. This is achieved by changing the `OSM_node_id` property of a particular node, which is stored in the network node data-frame, from the OSM ID to `charging_station`. Similarly, regular nodes with an arbitrary OSM ID ranging from 1 to 5 and one node hosting a CS, titled respectively, have been depicted in Figure 5.3a.

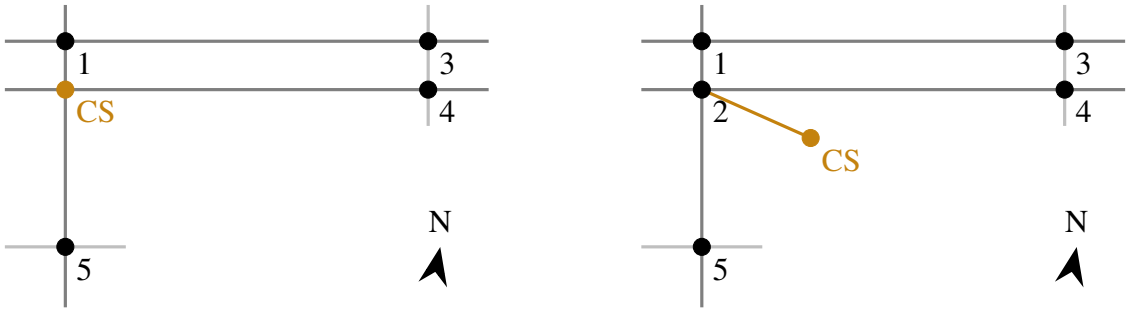

(a) Replacing the OSM id, which would have been 2 in this exemplar graph, of the junction at which CS is located in brown.

(b) An additional node for the CS is added, as well as a virtual access and exit road, both depicted in brown.

Figure 5.3 A graphical overview of the intuition behind the two methods of adding charging stations, depicted in red, to the OSM network model. An abstraction of

Both graphs in Figure 5.3 are based on the same real world example of Figure 5.1a, i.e. with the unconsolidated OSM network nodes for visual clarity and for validation through accessing OSM, namely the block group in Central Berkeley. This is done considering there is a Shell petrol station located along University Avenue, between Bonar Street to its west, which intersections represented by nodes 1 and 2, and Acton Street to its east, which intersections represented by nodes 3 and 4. Additionally, the station is only accessible when traversing through the southern intersection of the two on University and Bonar, since the link connecting nodes 2 and 4 is the unidirectional opposite of the link connecting nodes 1 and 3, these two links jointly represent University Avenue. Explanation on the OSM network and the underlying data, including the original OSM IDs, to this block group has been provided in Section A.2.

The raw origin-destination data is obtained from Replica, explanation on which is provided in Section 3.2, and converted into a data-frame with each trip representing a row containing both the origin and destination network node IDs, as well as the OSM node IDs, trip starting time, trip ending time. Setting the OSM ID property to the string value `charging_station`, allows for rerouting EVs by means of splitting an agents OD data into two, the first trip of which ends at the CS, whilst the second originates from the CS and ends in the original destination, i.e. the EV is charging on its route to the trip destination. Careful considerations go into setting the starting time

of this second trip, as it is to include a (potentially dynamic) waiting time as well as charging time at the CS. The additional benefit of setting the OSM ID attribute is that the underlying network model remains unchanged, preserving the benefits explained in Subsection 3.1.1.

Taking into account vehicles will have to cross the intersection that provides access to either the CS or its access roads anyway, it could be argued that the addition of new nodes and edges is considered redundant and vehicles are assumed to leave the network model when (waiting for) charging and re-enter the network for the second half of their trip, towards their original destination as explained in the previous paragraph, after the waiting and charging time have passed. However, agents leaving the network after arrival, implies infinite capacity at the CS, leading to unrealistic results in terms of downstream effects on congestion.

The goal of this research is to identify the influence of EVCS placement on traffic and to visualise the potential new bottlenecks caused by this induced demand. Keeping this in mind, the ABM fortunately is capable of modelling queues, in particular of queue backtracking since it will not allow vehicles to enter links once they are saturated. As an example for downstream effects of queues in the network I will use a traffic jam on University Avenue, then other vehicles will not be able to enter, which leads to queues on the roads leading up to University Avenue. Additionally, the model allows for extracting the arrival time of agents at their destination, hence allowing for dynamically setting the departure time of agent's trip from CS to destination.

In conclusion, for realistic modelling the effects of charging, the existing graph $G(V,E)$ as presented in Section 3.1, i.e. the ABM system input, is updated. A new network node $c \in C$, where the set of CSs is represented as $C \subset V' \supset V$, as well as an access $l(u,c) \in E'$ and exit "dummy" link $l(c,u) \in E' \supset E$, will be added for each additional CS that is added the network. The updated graph becomes $G'(V',E')$, it has $|V'| = |V| + |C|$ nodes, and $L := |E'| = |E| + 2 \cdot |C|$ edges. To account for charging time, the traversing time of $l(u,c)$ will be set to 30 minutes [54, 55].

5.4.1 Locations of direct current fast chargers in network

First, the existing DCFCs will be introduced in the network. Table 5.1 summarises the relevant information about the DCFC in the area of study: there currently is 1 DCFC operated by EVgo, with 4 ports in the area of study. The DCFC is located in Elmwood, Berkeley (Table A.2), its precise location on the map has been provided in Figure A.1. Provided the constraints on placements set by the electricity grid as touched upon in Section 1.3, locations will be selected based on potential locations at which the grid would be able to deal with the loads in Berkeley using the Micro-Siting Tool provided by the Pacific Gas and Electric Company (PG&E) [56]. Hence, this tool can be used

for obtaining permissible DCFC locations the extension of the public charging capacity through the introduction of new DCFCs.

Table 5.1 DCFC in the area of study, as depicted in Figure 3.1.

Power output	Ports	Street address
100 kW	4	3000 Telegraph Ave

When the number of potential locations is large, a study on the potential lessons from petrol refuelling for alternative fuel networks might be considered for selecting the locations. In this study, the authors concluded that the route between home and the nearest freeway entrance may aid with better predicting a large portion of spatial distribution of petrol demand compared to vehicle kilometers (read distance) travelled (VKT) [57], as demand for fuel increases near highways. They used a case study on the Sacramento, California, and describe optimal placement to cover spatial demand in an alternative fuel network using a river analogy, with initial stations located near highway entrances and subsequent ones placed more upstream, i.e. closer to peoples homes, as the market grows.

5.5 Charging demand

For estimating the demand for public charging, in line with the second sub-question as listed in Section 4.2, the Electric Vehicle Infrastructure Projection Tool (EVI-Pro) may be used [58], as has been done in previous research [59]. This tool requires the following inputs for estimating DCFC demand: the total number of PEVs in the fleet, the average daily VKT, the number of PEVs in the fleet that are all-electric, i.e. the share of BEVs, and ambient temperature. In the following section, the inputs will be listed as it will prove useful not only for this tool but also for simulation purposes.

For Alameda County, i.e. the greater Berkeley area containing all considered zip codes from Table A.2, in the autumn of 2021, these inputs are 8.140 PEVs (6.96% of the total car population) [60], 25 miles (40 kilometers) per day [58], 74.3% [60] and 60 degrees Fahrenheit (15 degrees Celsius) [61] respectively. An example of the resulting charging demand for plugging in these values into the EVI-Pro tool has been provided in Section A.4. It should be noted that the peak DCFC demand from Figure A.2 approximately corresponds to the maximum charging capacity with the 4 chargers of 100 kW each (Table 5.1) provided the current, or historic, i.e. from autumn 2021, level of EV penetration of approximately 7%.

Note that public chargers are not used predominantly as of 2021. Currently, approximately 80% of EV charging happens at home [62], this is however expected to change in the future, with more

people adopting to the use of EVs without access to residential chargers. In the EV driver survey conducted by Plug In America that had over 3,500 respondents, of which 83% reportedly owned a BEV, 2% of the respondents predominantly used public DCFCs and 92% prefer home charging over any other type of charging [63]. Additionally, 47% reported using DC fast charging daily or weekly. In conclusion, the number of EVs which in reality charge at the DCFC on Telegraph is likely to be smaller than the entire EV population of 7%: according to [64], 5% of the 7,980 BEV charging trips within their study area in California take place at DCFCs, answering to the fourth research sub-question as listed in Section 4.2.

6

Agent based model validation

This chapter is intended to provide insight into how representative results from ABM simulations prove to be, therewith answering to the eighth research question, i.e. how this model might aid in bottleneck identification. When simulation results prove to approximate real world traffic to an acceptable extent, the ABM can indeed be used to identify new bottlenecks resulting from charging trips. Initial performance of the ABM is therefore evaluated through comparison of simulated trip arrival time actual arrival times from the OD data for a 24 hour typical Thursday in the autumn of 2021. In sections thereafter, the effect of rerouting on the accuracy of simulation results will be provided, as well as a sensitivity analysis of model parameters which might allow for model calibration to better approximate real world traffic.

6.1 Initial performance

As can be seen in Figure 6.1, there is high variation in terms of relative trip duration difference, especially in terms of simulation trips that take much longer, ranging up to a 26,100% increase. The horizontal axis of the figure corresponds to the agent IDs in the simulation, these range from 0 to 176,000 trips, in accordance with Section 5.1. When looking at the distribution of all percentage error values, in particular the left plot of Figure A.3; a zoomed view of which is provided in Figure 6.2a, the share of outliers in the distribution seems much smaller when comparing to Figure 6.1, the single narrow spike in the histogram located around 0% confirms that 99.9% of all trips actually have a percentage error, between negative and positive 100%.
According to the right plot of Figure A.3, most simulated trips arrive earlier than the actual trip, i.e. simulated trips which have a percentage difference within -100% and 0%, with the mode being around -38.7%, as can be seen in Figure 6.2a. This could be justified by the statements in Subsection 5.1.1.

A mean (absolute) percentage error measure (MPE or MAPE) can be used on the arrival time of

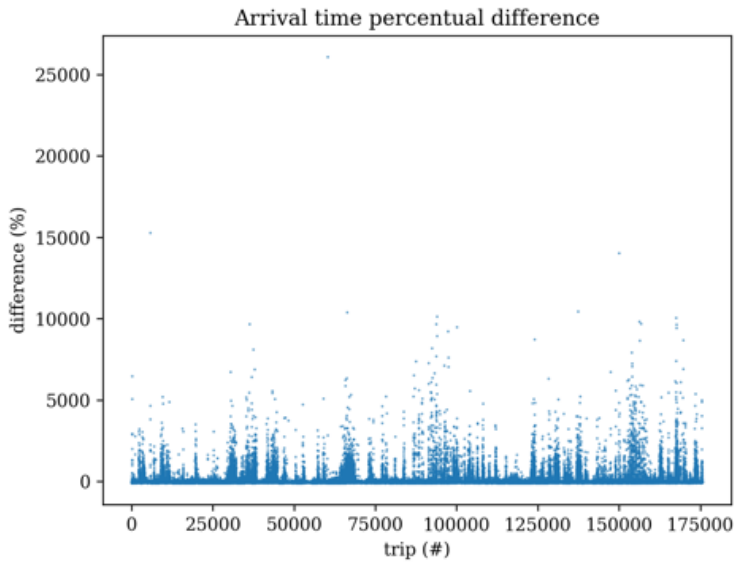

Figure 6.1 Percentage difference in trip duration for all agents for the simulation of autumn 2021.

simulated and actual trips as it is considered a good choice for evaluation of model accuracy when the value of data is large which is the case here, as the value of time is measured in seconds [65]. For the autumn data of 2021, the MPE in trip duration is 39.2%. This entails that on average, simulation trips take around 1.4 times as long. The MAPE is equal to 118%. Considering that the mode of all percentage errors is equal to -38.7%, the distribution has a rather long right tail with outliers, influencing the average percentage error. Concluding, on average for the autumn 2021 scenario without rerouting, an actual trip of 5 minute may take about 7 minutes on average in the simulation using the MPE. The mode of 5 minute long trips take approximately 3 minutes.

There are two reasons for explaining the rather large MAPE, one of which is that some trips get stuck in queue after queue in the model, causing the large right tail of the distribution. For the purpose of saving computational time, the rerouting frequency is set to equal the simulation time, this limits the number of calls to the shortest path algorithm, or the function call (b) in Figure 3.4. Therefore, the shortest path calculation will only be performed once, at the beginning of the simulation, and agents will not try to avoid queues which suddenly appeared causing some trips to take. Another reason is that MAPE has the significant disadvantage that it produces infinite or undefined values for zero or close-to-zero actual values [66], i.e. very short trips.

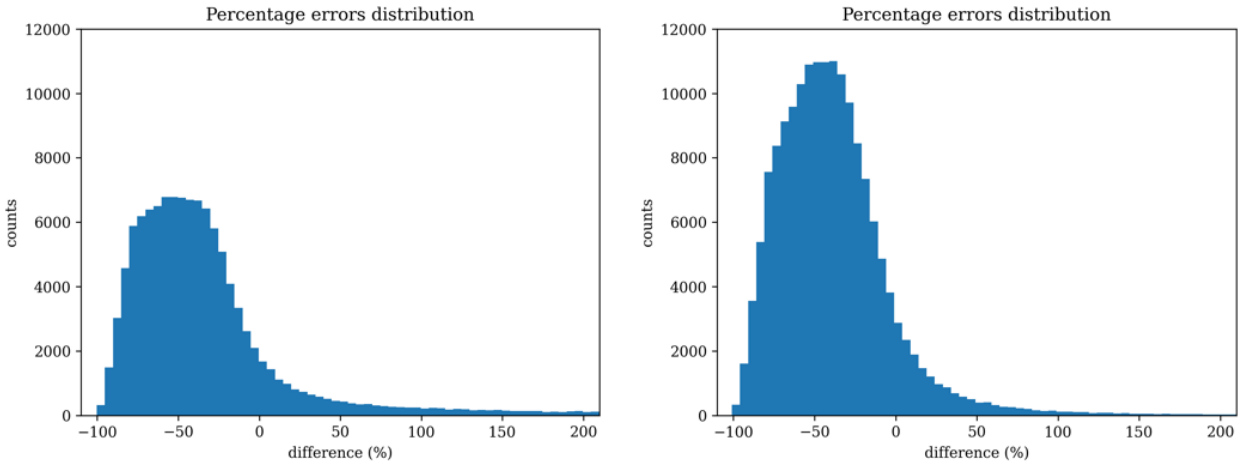

(a) Base simulation without rerouting. **(b)** Simulation with rerouting every 5 minutes.

Figure 6.2 Zoomed view of the percentage error distribution of simulation and actual trip times with autumn 2021 demand data, containing both negative and positive values, plotted on the same axes.

6.2 Rerouting

Changing the rerouting frequency from never to every 5 minutes results in a huge improvement of M(A)PE for both scenarios. For fall 2021, the MPE is equal to -38.8% and the MAPE is equal to 46.8%. Hence, trips that actually take 5 minutes on average take 3 minutes when rerouting is allowed, which is very similar to the aforementioned mode of the percentage error and thus more representative for the distribution of percentage error. Hence, when rerouting is allowed in the model, a large number of error outliers is prevented since agents will not stay stuck in traffic but figure out a new route instead. As can be seen in Figure 6.2, the simulation where rerouting is allowed results in a distribution which is more centered around its mode as can be seen in Figure 6.2b; the histogram shows higher counts around the mode and a much smaller right tail of the distribution.

Allowing vehicles to reroute might however lead to fluctuating network performance: since vehicles may reroute to roads that seem fine currently, causing instantaneous blockage, a well-known property of physical-queue traffic models, such as Zhao's ABM, which also happens in reality. This sudden blockage can lead to substantial changes in the route travel times, even with a small change in the flow pattern [67]. This implies that the current shortest route can become an unacceptable route in the next iteration, more aggressive swapping behavior hence might cause oscillations in network performance. Zhao's model accounts for this purpose by updating the travel time of each link with the time that vehicles which left the link in the past 60 seconds experienced, i.e. it is a

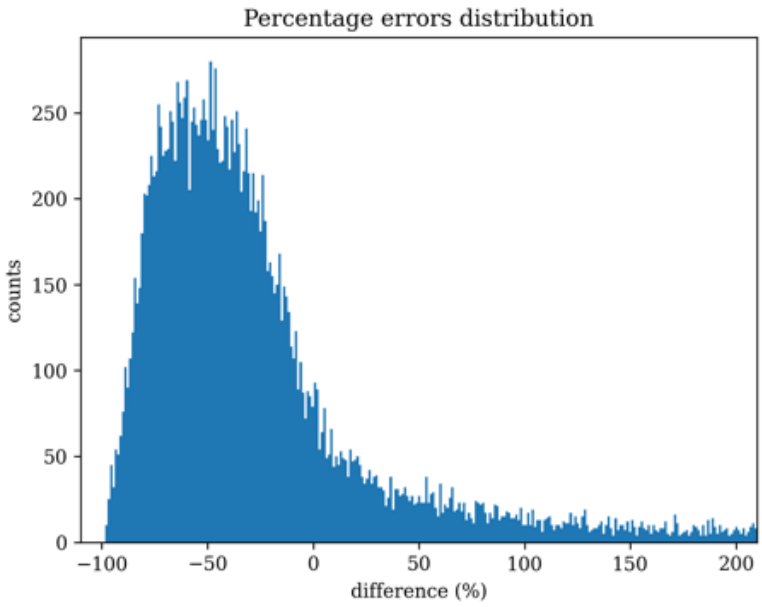

Figure 6.3 PE in trip duration for all agents present in the simulation of the autumn 2021 afternoon rush hours, 4 p.m. to 6 p.m., on a typical Thursday.

moving average of all vehicles that just left the link which is known to smooth fluctuations [68, 69].

6.3 Sensitivity analysis and calibration

The effect, or sensitivity, of both parameters, as listed in Subsection 5.1.1, on simulation arrival times will be analysed in this section with the ultimate goal being to mimic the effect of background traffic and hence, obtain simulation arrival times that better approximate the data. Figure 6.3 shows the PE distribution of the simulation of afternoon rush hours from 16:00 (4 p.m.) to 19:00 (6 p.m.), which closely matches the distribution profile of Figure 6.2a but with less data points. The focus of this calibration process is mostly on adjusting the parameters starting from the slowest links first. As fully rational agents choosing the shortest path might then be discouraged to take small residential streets and rely more on the primary, higher capacity roads to reach their destination. The model assumes that agents are able to cross links on the speed limit as explained before. However, the model does not account for the presence of stoplights and signs, nor speed bumps that reduce the average link traversing speed.

6.3.1 Link speed

The first adjustment is to change the speed on network links. Note that the speed of different type of links can be adjusted separately, e.g. residential or motorway (freeway), labels that indicate road types obtained from OSM. The parameters of the researched scenarios have been listed in Table 6.1, the speeds are provided in mph for the Berkeley case study, this can easily be adjusted to kph for studies in regions where the metric system is used predominantly. Figure 6.4 provides a visualisation of the PE distributions after changing the speed limit on residential links, depicted with SR in the scenario name, and primary links, depicted with SP in the scenario name. Figure 6.4a shows a more widespread distribution centered more closely on 0% difference. The addition of the link speed reduction of the primary links seems to reduce the number of the highly negative PEs, as can be seen in Figure 6.4b, this alone does not really affect the distribution and is contrary to the previously stated, namely that it discourages agents to use higher-capacity roads.

Table 6.1 Link speed per scenario for every road type. Note that road type "Other" includes residential streets. In the scenario titles, SR entails speed of "Other" road types and SP entails speed of primary roads.

Link type	Base	SR10	SR10SP35
Motorway	65 mph	65 mph	65 mph
Primary	55 mph	55 mph	35 mph
Other	25 mph	10 mph	10 mph
Figure	6.3	6.4a	6.4b

6.3.2 Link capacity

The second parameter investigated for its sensitivity is link capacity, which refers to the number of vehicles that the link can carry in one hour. The parameters of the researched scenarios for link capacity have been listed in Table 6.2. Figure 6.5 provides a visualisation of the PE distributions after changing the capacities on residential links, depicted with CR in the scenario name, and primary links, depicted with CP in the scenario name. Figure 6.5a shows a more widespread distribution, due to which it appears to center more closely around 0% difference. The addition of the link capacity reduction of the primary links seems to only reduce total counts of the PE histogram, judging from the vertical axis of Figure 6.5b, and not change the shape of the distribution much. Further decreasing the capacity of residential streets results in an even less favourable PE distribution.

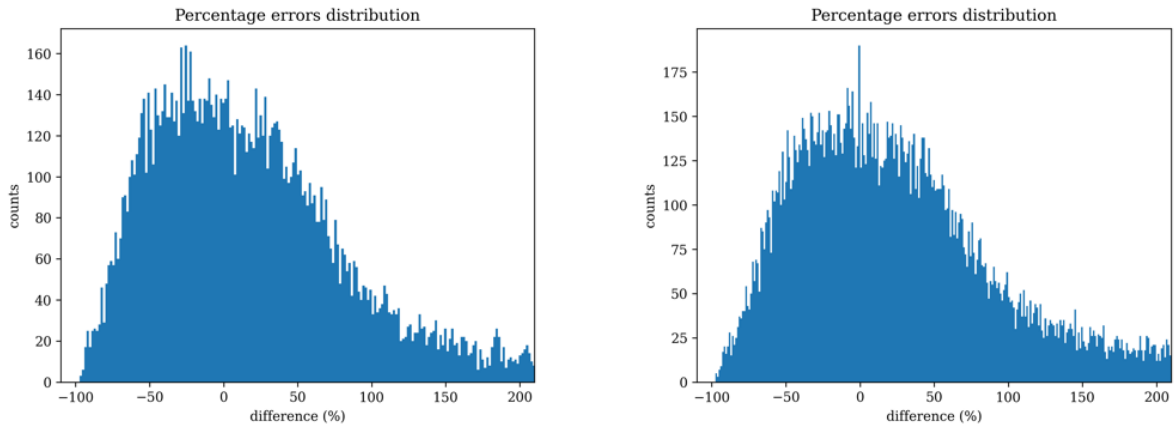

(a) SR10 scenario. **(b)** SR10SP35 scenario.

Figure 6.4 PE of trip duration in the afternoon rush hours simulation with different link speeds for the "Other" (SR), and primary links (SP).

Table 6.2 Link capacity per lane of every road type and for every scenario. In the scenario titles, CR entails capacity of "Other" road types and CP entails capacity of primary roads.

	Base	CR450	CR450CP800
Motorway	2,350 veh/h	2,350 veh/h	2,350 veh/h
Primary	1,200 veh/h	1,200 veh/h	800 veh/h
Other	950 veh/h	450 veh/h	450 veh/h
Figure	6.3	6.5a	6.5b

In conclusion, adjusting the link speed, in particular of residential street seems to have the desired effect of getting the PE more centered around 0%, adjusting the capacity does not. Hence, if the model is used for simulations, calibration can be used to obtain more realistic approximations in terms of arrival times. However, it must be noted that especially the right tail of the distribution, i.e. the simulated agents that arrive (much) later than actual ones in data, becomes larger. This statement is backed by the data provided in Table 6.3, as can be seen, there is a major increase in M(A)PE after calibrating parameters to slow down traffic. Calibration does seem to have a positive effect of moving the mode.

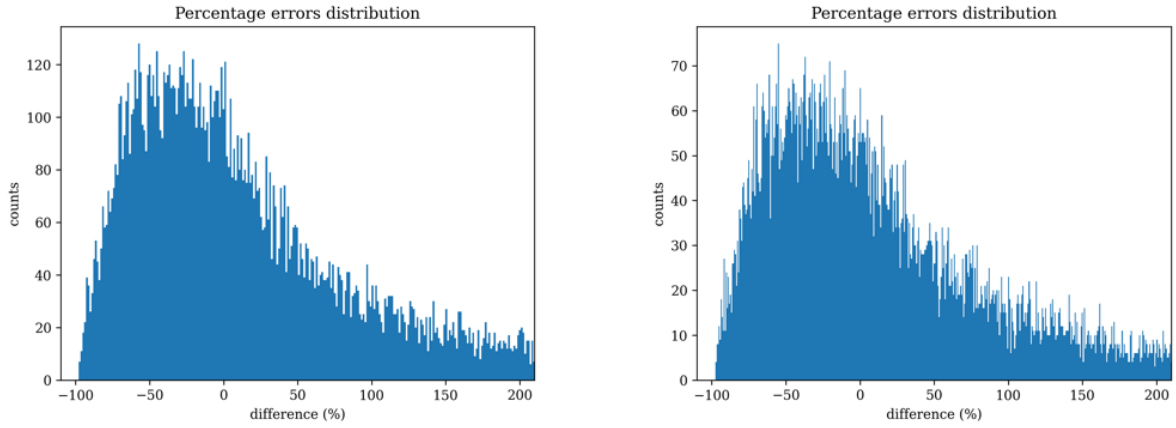

(a) CR450 scenario.

(b) CR450CP800 scenario.

Figure 6.5 PE of trip duration in the afternoon rush hours simulation with different link capacities for the "Other" (CR), and primary links (CP).

Table 6.3 M(A)PEs of the arrival times belonging to the previously provided distributions compared to the actual agent arrival times from the Replica OD data.

	Base	SR10	SR10SP35	CR450
MAPE	-5.95%	66.3%	61.3%	105%
MPE	64.7%	91.8%	86.6%	142%
Mode	-48.5%	-25.5%	-0.561%	-57.2%
Figure	6.3	6.4a	6.4b	6.5a

7

Dynamic traffic assignment

Section 3.4 briefly touches upon the route choice of agents, through the Dijkstra inspired sp algorithm, as well as the link travel time update rules. This chapter elaborates on how the traffic network updates during the simulation and the mathematical interpretations of link and agent travel times in the first section. Additionally, explanation is provided on equlibria in time-varying queue models and the implication on simulation results and the last section puts forward formulations to describe the agent's route choice within the network and makes these choices insightful.

7.1 Travel times

Let $\Phi_l(z_l(t)) \; \forall \; l \in E'$ denote the non-decreasing link travel time, or delay, function depending on the current link flow $z_l(t)$ in vehicles per hour. Note that l here is used to denote a link for simplicity, as explained in Subsection 3.1.1. In theoretical papers, $\Phi(z)$ is often equal to the power function from the Bureau of Public Roads (BPR) [70, 71]. It should however be noted that the BPR function allows for flows higher than the physically possible link capacities [72]. Zhao's ABM is a so-called physical queue model, which entails that it has finite storage capacity due to which the end of the queue spills back onto preceding links [67]. Effectively, it entails that the ABM does not allow more vehicles to enter the link, in contrast to BPR, when the total length of all queued vehicles on that link minus the total link length is smaller than the length of one vehicle, this represents real-world behaviour but might result in the non-existence of solutions to the dynamic traffic assignment (DTA) problem [67]. DTA deals with assigning traffic volume onto a dynamic, time-varying, traffic network with a specified demand [73].

In order to study the (dis)continuity of link travel time in the ABM in discrete time $t := [t_0, T]$, I let the `simulation_queue.py` output additional data-frames that store the current flow and delay time for all links in the network which are currently occupied, i.e. for any number of vehicles using the link. Now, in order to relate the right values with one another, i.e. the agents actually

causing the delay with the delay time that they experienced, a 60 second moving average of the link capacity is taken, the code to accomplish this has been provided in Section B.2. This is done to match the link travel time, which is also a 60 second moving average as mentioned before. Note that delay time $d_l(z_l) := \Phi_l(z_l) - \Phi_l(0)$, where $\Phi_l(0)$ is the link free-flow time, is plotted instead of link travel time to set a baseline (zero) for all links because links have different free-flow times, as these depend on their speed limit and link length. A scatter plot of this data, for both residential streets and primary roads, has been provided in Figure 7.1. The figures are obtained with the same simulation set-up as used in Chapter 9, i.e. of the morning rush hours from 6 a.m. to 10 a.m. with cool-down where rerouting is allowed, explanation on which is provided in Chapter 9. Curve fitting could potentially be used to obtain a (continuous) function that best describes the relationship between flow rate and delay time. It can however not be guaranteed that the link delay functions always behave according to this fitted function. Concluding from the figures, residential streets seem to generate extreme queuing, with nearly 5 hours of waiting experienced by one vehicle as compared to the primary roads with higher capacity, where agents experience a delay of at most 3 minutes.

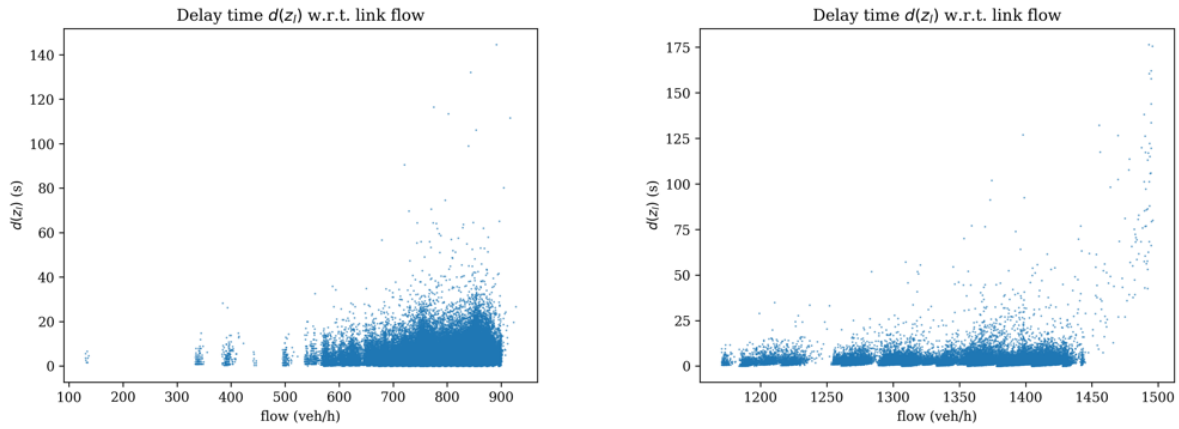

(a) Delay time on residential streets, capacity 950 vehicles per hour.

(b) Delay time on primary roads, capacity 1500 vehicles per hour.

Figure 7.1 Scatter plot of link delay time (seconds) w.r.t. flow (vehicles per hour).

7.2 User equilibrium

When the link travel time function $\Phi_l(z_l)$ is continuous with respect to traffic flow z on link l, a user equilibrium (UE) exists in static transport networks [74], when $\Phi_l(z_l)$ is also strictly monotone,

i.e. for $\Phi_l(x) > \Phi_l(y)$ when $x > y$, this UE is unique [75, 76] and known as the first principle of Wardrop for traffic assignment in a road network. The principle states that all route choices have the same travel cost and this cost is not greater than the travel cost of unused options between each OD pair [77], i.e. agents do not gain by unilaterally changing route. For this reason, it is desirable to have a continuous link delay function, it allows to study optimal states in the network which are achieved by agents minimising their travel time.

This concept of UE has been applied in DTA. In order to ensure the aforementioned requirements of UE, theoretical studies often assume continuous delay functions to describe the link travel time for queued vehicles resulting in point queues [67, 78], e.g. using a step-wise delay function which is linearly increasing when the current demand exceeds capacity and zero otherwise [79]. Point queues usually have constant downstream service rate, or exit flow, and the infinite storage capacity [80], whereas physical queue models have the aforementioned spill-back property, potentially causing discontinuous route travel times w.r.t. route flows, which violates the condition that ensures UE existence [74, 81, 82].

7.2.1 Dynamic user optimum

More recently, experts in the field adopted to using the notion of dynamic user optimal (DUO) state [83] to capture 'stable' states even when continuity of path travel costs is not guaranteed. The aforementioned article categorises the notion of DUO in previous research by their degree of tolerance, a measure that bounds the deviation for the used paths of the same OD pair, i.e. the actual experienced travel time minus the shortest travel time over all possible paths of OD pairs at time t. In that respect, a strict DUE would be similar to a DUO with zero tolerance. The mathematical expression of an agent's payoff, relating it to the link travel times depends on the route choice. Route choice is summarised in a routing matrix R, where entries for path i and link l, read:

$$r_{il} = \begin{cases} 1 & \text{if } l \text{ in path } i \\ 0 & \text{otherwise} \end{cases} \tag{7.1}$$

and the matrix, $R \in \mathbb{R}^{N \times L}$, reads as

$$R = \begin{bmatrix} r_{11} & r_{12} & \cdots & r_{1L} \\ r_{21} & r_{22} & \cdots & r_{2L} \\ \vdots & \vdots & \ddots & \vdots \\ r_{N1} & r_{N2} & \cdots & r_{NL} \end{bmatrix} \tag{7.2}$$

where each row correspond to a path $R_{i*} \in \mathbb{R}^L$. Consequently, the payoff of all routes $F(z) \in \mathbb{R}^N$, can be expressed as a function of the agent's path occupancy, or flow:

$$F(z) = -R\Phi(z) = -R \begin{bmatrix} \Phi_1(z_1) \\ \Phi_2(z_2) \\ \vdots \\ \Phi_L(z_L) \end{bmatrix} \tag{7.3}$$

where the payoff equals negative travel time for a particular path, i.e. the larger the travel time, the lower the payoff. This is done for intuitive payoff understanding. Note that travel cost incurred by agents in DTA travelling on the same path however are not necessarily constant due to the change in link flows and resulting link travel costs over time. This likely differs between rush hours and off-peak periods.

7.3 Route choice

The route choice problem is solved by all agents selfishly maximising their payoff, i.e. minimising their travel time. Two agent types are considered to model charging behaviour for defining route profiles, namely EVs that use a DCFC on their trip (the vehicle type of these in the demand data will be set to EV as explained in Section 8.1), e.g. due to a low battery level, and all other vehicles, e.g. agents with internal combustion engine vehicles (ICEVs).

Since agents with BEVs, or type 1, are to charge on their trip, their route is to include one CS access and exit link, $l(u,c)$ and $l(c,u)$ respectively or $r_{l(u,c)} = 1$ and $r_{l(c,u)} = 1$, where u is a network intersection that provides access to the CS, $c \in C \subseteq V'$. However, since EV trips are split up into two their routes automatically include the DCFC links, as these will be the last link of their first trip and first link of their second trip. Therefore, I will not dive into the set of available routes to agents. Note that the CS access link encompasses the charging action and includes charge time as has been mentioned in Section 5.4 so waiting time is accounted for when picking route R_{i*}.

Path choice translates to payoff in the following way: the routing matrix is multiplied with the decision variables stored in matrix $X \in \mathbb{R}^{K \times N}$ for a total of K agents. Each row of this matrix $X_{k*} := \begin{bmatrix} x_{k1} & x_{k2} & \cdots & x_{kN} \end{bmatrix}$ represents the choice of route i for agent k, its elements are binary $x_{ki} \in \{0,1\}$ and multiply with all L columns of R. This entails that XR results in a $K \times L$ matrix which rows represent the links present in the path of agent k. As stated before, agents can only choose routes that include their origin and destination. Hence, the set available decision variables to agent k, denoted by χ_k, are all paths that connect origins O to destinations D, all decision

variables for other paths equal 0:

$$x_{ki} = \begin{cases} x_{ki} & \text{if} \quad r_{il(O,u)} = 1 \wedge r_{il(v,D)} = 1 \\ 0 & \text{otherwise} \end{cases} \tag{7.4}$$

and the sp algorithm takes care of this [47].

7.3.1 Objective function

Route choice is affected by link delay, which changes over time because of agents moving through the network and new ones spawning, this directly affects the payoff at time t in accordance with Equation 7.3. Provided this time-dependence and the previously presented route choice formulation with variable X, the objective function for all agents departing at time t is equal to

$$\begin{aligned} U(X,t) &= XF\left(z(t)\right) \\ &= -XR\Phi\left(z(t)\right) \\ &= -\begin{bmatrix} x_{11} & x_{12} & \cdots & x_{1N} \\ x_{21} & x_{22} & \cdots & x_{2N} \\ \vdots & \vdots & \ddots & \vdots \\ x_{K1} & x_{K2} & \cdots & x_{KN} \end{bmatrix} \begin{bmatrix} r_{11} & r_{12} & \cdots & r_{1L} \\ r_{21} & r_{22} & \cdots & r_{2L} \\ \vdots & \vdots & \ddots & \vdots \\ r_{N1} & r_{N2} & \cdots & r_{NL} \end{bmatrix} \begin{bmatrix} \Phi_1\left(z_1(t)\right) \\ \Phi_2\left(z_2(t)\right) \\ \vdots \\ \Phi_L\left(z_L(t)\right) \end{bmatrix} \end{aligned}$$

where $U \in \mathbb{R}^K$ denotes the payoff vector for all agents, in contrast with $F \in \mathbb{R}^N$, which is the payoff for all routes. As stated, $XR \in \mathbb{R}^{K \times L}$ and hence, multiplication with $\Phi \in \mathbb{R}^L$ results in $U \in \mathbb{R}^K$.

This formulation is more fit for use as an objective function because the decision variable is a direct input to it. Note that even though agents cannot choose their departure time, their route choice depends on the current link occupation and hence, U is a function of X and t.

7.3.2 Simulation

As explained before, agents observe the traffic network right before they depart, as they will check total travel time. For agents with BEVs, this includes wait and charge time in line with Section 8.1. Their payoff is $U_k(X_{k*},t)$ and depends on the chosen path as well as choices path choices of all other agents that consequently influence link flows $z_l(t)$, i.e. agents with other OD pairs traversing over the shared links, as many paths may share roads. Therefore, links may become congested due to road occupation by other agents who end up at links shared among routes that made the route choice based on the travel times in the past. The problem in the previous sections is converted

into a binary integer program (BIP). The objective function to be optimised through a route choice before departure taking into account current link travel times:

$$\begin{aligned} \underset{X_{k*} \in \chi_k}{\text{maximise}} \quad & U\left(X_{k*}, t\right) = -X_{k*} R \Phi\left(z\left(t\right)\right) \\ \text{subject to} \quad & \sum_{i=1}^{N} X_{ki} = 1 \\ & x_i \in \{0,1\} \forall i \end{aligned} \tag{7.5}$$

The objective function in Equation 7.5 represents the payoff for one agent, k, who must choose only one path from the paths that connect their origin and destination, i.e. from the set χ_k, this is enforced through the first constraint. This objective function is applicable both in the case when rerouting is allowed and when it is not, in the case of rerouting the same optimisation is done, agents observe the network at a different time-step and then choose among the paths that connect their current node with their destination. In the simulation, this is achieved through the function call to `get_path()`, which is in the Agent class. This function does an actual call to Dijksra's sp algorithm in line with arrows b and c in the system description and outputs the shortest path. Accordingly, the agent's path, which is an array of nodes that are to be traversed through, is updated corresponding to the new order of nodes.

Because of the statements in Section 7.2, it may not be guaranteed if UE is achieved in the ABM. It is assumed that agents individually minimising their travel time on the same points in time leads to a DUO. As DUO exists for models that exhibit queue spill-back, this optimum hold in the bounded (maximum value of link delay time) solution space. Future research is to establish stricter bounds for DUO to achieve solution uniqueness, this is currently not guaranteed.

8

Charging demand assignment

In the previous chapters, the system, its boundaries and the methodology for the integration of Zhao's ABM with real-world inputs from the city of Berkeley, the model's validation and mathematics have been established. This chapter will be devoted to the major contribution of this research project, namely modelling charging demand and studying the induced demand on the traffic network using Berkeley as a case study. This chapter will answer to the fifth research sub-question, as different DCFC placement locations will be proposed.

To get insights in induced demand, charging trips have to be added to the OD demand data, in line with the previously stated in the third paragraph of Section 5.4. To position this chapter in the system of this research, it is part of the input side to the ABM, as it concerns complementing the demand data, from Section 3.2, with charging trips. The challenge is to determine which agent will charge and if they decide to, when and where they do. It is worth noting that throughout this chapter only charging trips to public DCFCs are considered. Additionally, only BEVs are considered since PHEVs cannot be charged at DCFC stations [84] and, in accordance with Section 5.4, charging time is considered a constant of 30 minutes.

In the following sections of this chapter, several policies, or scenarios, for DCFC placement are presented. These sections cover the reasoning behind, as well as the implementation of all scenarios. It is assumed that the adoption of BEVs will keep increasing due to governmental incentives, for the area of study this is the earlier mentioned legislation issued by the State of California [11], an additional 3 DCFCs will be placed in the city in all investigated scenarios.

For simulation time purposes, morning rush hours are considered, i.e. demand data of all trips that start between 6 a.m. to 10 a.m. to start with a near empty network Figure 3.3. The simulation will be given a 3 hour cool-down period where new demand is cut-off to let the agents that are currently travelling through the network finish their trips. Hence, the demand peak of the morning

rush hours, in line with Figure 3.3, is isolated and studied. Additionally, it is assumed that agents revise their route each 2 minutes, to avoid getting stuck in queue after queue, as it is highly unlikely that agents will be willing to stay queued in inter-city traffic without considering alternative routes, meaning that they do not consider rerouting, e.g. from the arterial roads that might be jammed for a while.

8.1 Demand data preparation

A step-by-step guide on how charging trips are added to the OD data has been listed below.

1. OD demand data is created using a Replica csv file.
2. A particular percentage is requested as an input to correspond with the random proportion of the cars that are EVs, in the case study of Berkeley in autumn 2021 and in line with Section 5.5, this is approximately 7%.
3. Either all or a proportion of the EV trips in the demand data are duplicated once, resulting in two trips from the same trip taker.
    (a) The destination of the first, or original, trip becomes the geographically closest, i.e. using the Haversine function, DCFC obtained. This results in a DCFC origin distribution such as in Figure 8.1 and C.1. This trip's origin and departure time are left unchanged.
    (b) The origin of the second, or duplicated, trip becomes the CS that the first trip has as destination. This trip's destination is the original trip's destination and is therefore unchanged.
    (c) Departure time for the second trip depends on the arrival time of the first to the CS. Hence, for initialisation this value is not a number (NaN).

All agents that decide to charge at a public DCFC, i.e. all BEV trips in the the OD data are split into two and visit a DCFC, and check its current availability. This entails that, a couple seconds before the departure time of an agent's charging trip, the agent observes the traffic network state, e.g. through the use of applications that provide insight in the current status of the road network in terms of travel times such as Waze, EVgo or Google Maps, to check their travel and waiting time for different stations.

Since it is assumed that all agents are selfish and maximise their own payoff, i.e. minimising their additional travelling and waiting time, for selecting a DCFC. This is achieved by calling the sp algorithm in `simulation_queue.py` therewith providing the agent's origin node ID, destination

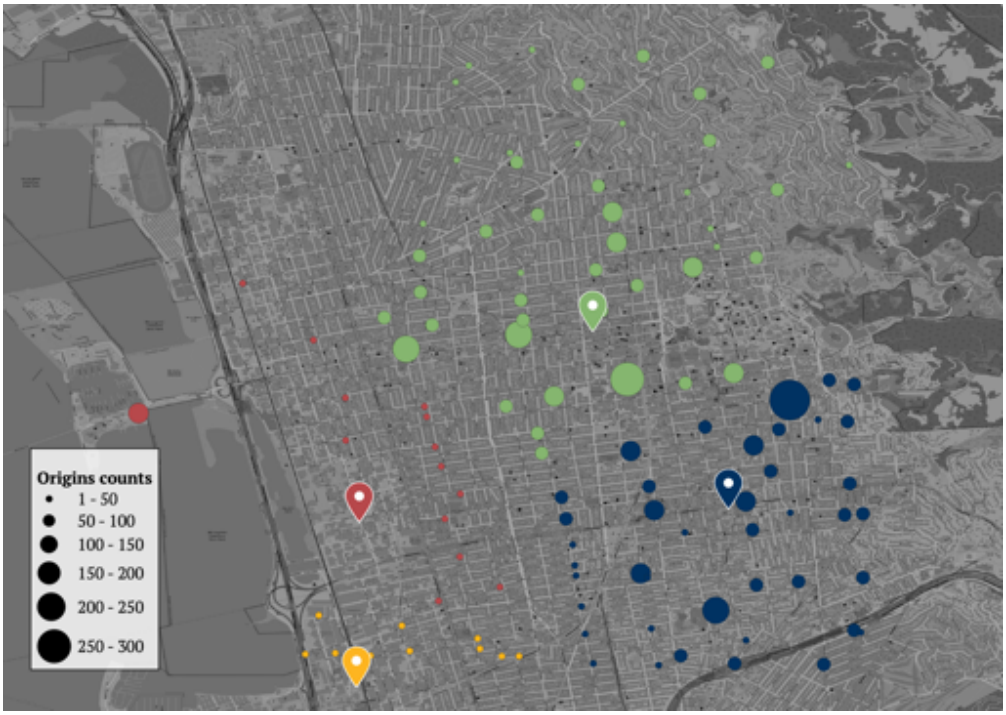

Figure 8.1 Geographical representation of origins and their counts for all EV trips in scenario 1 going to the geographically closest DCFC in Berkeley, i.e. the existing DCFC at 3000 Telegraph Avenue (blue) and to the newly added DCFCs on 1966 University Avenue (green), 2830 Seventh Street (red) and 5800 Shellmound Way (yellow).

node ID and the set of CSs in the network (O,D,C). Section B.1 lists the code for the function that achieves this purpose, note in particular the corresponding inputs. The sp algorithm will find the shortest travel time from origin O to destination D for all possible paths leading to and from each CS $c \in C$ resulting in an array of length $|C|$ for every BEV driver, `sp_dist` in Section B.1. Consequently, the index of the smallest value is found and used to output the index of the CS that adds minimum waiting and charging time, `closest_cs`, step 3(a) and (b) of Section 8.1 are accordingly repeated with the updated DCFC location.

Note that waiting time is included in the network through queue spill-back. These queues add to the agent's expected travel time and will be considered in their route choice. Moreover, the traversing time of the "dummy" link to reach the DCFC incorporates charging time. Therefore, choosing the DCFC with shortest travel time also allows for minimisation of agent's waiting time.

8.2 Scenario 1: spatial separation

Table 8.1 provides potential locations for future DCFCs in the area of study with rather large spatial separation (Figure 8.1), in an attempt to cover the charging demand across the city. Note that all locations have been selected for their sufficient excess transformer capacity according to PG&E's Micro-Siting Tool [56], i.e. at least 4 charging ports and preferably more due to the age of PG&E's data.

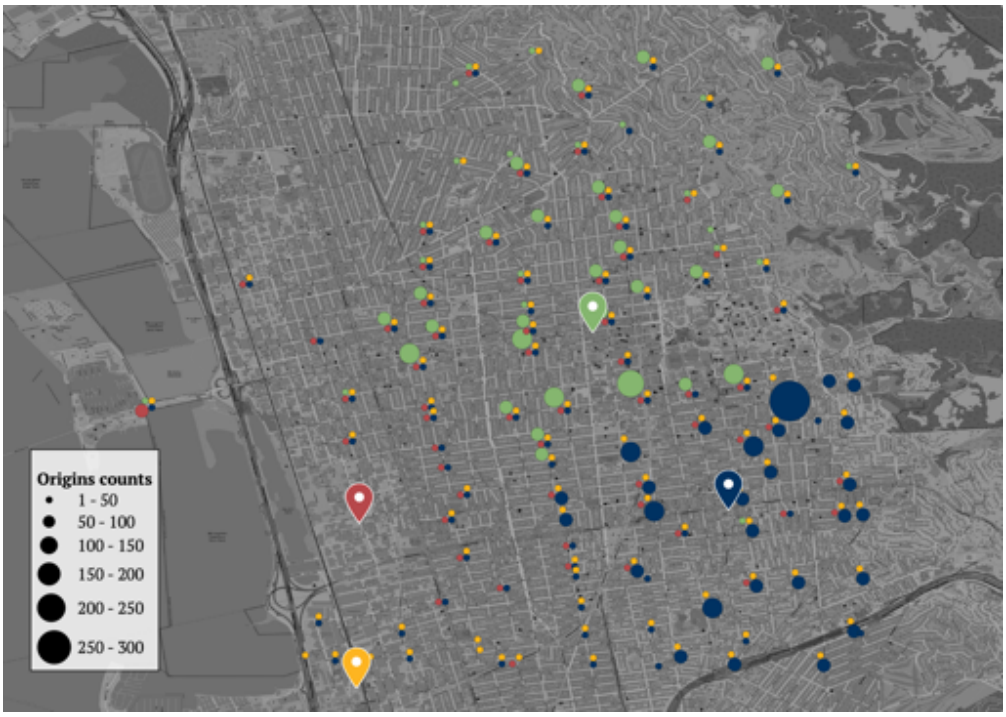

Figure 8.2 Geographical representation of origins and their counts for all EV trips going to a DCFC in Berkeley along the sp to their destination, in scenario 1.

Table 8.1 Potential locations for new DCFCs in the area of study for scenario 1, as depicted in Figure 8.1, along with the excess transformer capacity in terms of number of DCFCs that can be served.

Street address	Excess capacity
3000 Telegraph Ave	0 DCFCs
1966 University Avenue	35 DCFCs
2830 Seventh Street	53 DCFCs
5800 Shellmound Way	15 DCFCs

Initialisation of the charging trip destinations happens in line with the third bullet point of Sec-

tion 8.1 the geographically closest DCFC is selected, a visual representation of which is provided in Figure 8.1. The figure shows the cumulative number of origins from a simulation of a typical Thursday in autumn 2021 when assigning the charging trips to the geographically closest DCFC. Figure 8.2 provides a visual representation of the cumulative number of origins after updating the DCFC locations during the simulation provided the current traffic conditions according to Section 8.1. The data for Figure 8.2 was outputted after simulation, as the DCFC choices depend on traffic conditions which vary over the simulated time.

8.3 Scenario 2: close to demand

Table 8.2 provides potential locations for future DCFCs in the area of study for the second scenario, where DCFCs are placed closely to the high traffic demand, i.e. in the brightest areas of Figure 3.2. The resulting placement has been depicted in Figure C.1, figures for scenarios 2 and 3 are provided in the appendix since it comes down to the same principle of scenario 1. All locations have again been selected for their sufficient excess transformer capacity.

Table 8.2 Potential locations for new DCFCs in the area of study for scenario 2, along with the excess transformer capacity in terms of number of DCFCs that can be served.

Street address	Excess capacity
3000 Telegraph Ave	0 DCFCs
2150 Shattuck Avenue	27 DCFCs
1966 University Avenue	35 DCFCs
2001 Dwight Way	8 DCFCs

8.4 Scenario 3: clustering

Table 8.3 provides potential locations for future DCFCs in the area of study for the second scenario, where DCFCs are placed close to one another, like some petrol stations on an intersection or shops in a shopping mall. Resulting placement has been depicted in Figure C.2, the additional (to the existing on 3000 Telegraph Ave) 12 ports have been located at 2850 Telegraph Ave all in the same place.

Table 8.3 Potential locations for new DCFCs in the area of study for scenario 3, along with the excess transformer capacity in terms of number of DCFCs that can be served.

Street address	Excess capacity
3000 Telegraph Ave	0 DCFCs
2850 Telegraph Ave	13 DCFCs

9

Results

This chapter will present the results of the simulations having implemented all methodological considerations from the previous chapters. The first section will summarise the simulation parameters, for reproduction purposes in future studies. The second section will be devoted to the results of placement according to the scenarios discussed the previous chapter, i.e. the induced demand that results from placement according to the proposed placement policies as explained in Chapter 8. Results are provided in terms of queuing time difference between the scenarios and the base case, i.e. without modelling the intermediate charging destinations. The third section will provide results of scenario comparisons.

9.1 Simulation parameters

As stated before, the charging time is set to 30 minutes, or 1800 seconds, and an additional 3 DCFCs (4 in total), having 4 charging ports each, have been placed in the traffic network in all scenarios other than the base case. Moreover, all trips that depart between 6 a.m. and 10 a.m. are considered, this results in an approximate 20,000 trips through the network, of which there are approximately 1,400 BEVs, i.e. 7% of all vehicles. The demand data also exists of the BEVs second trips, i.e. the trips that go from the DCFC to the destination, which departure time after initialisation is set to NaN. After an agent arrives at a DCFC, the departure time of their second trip will be set during the simulation. Therefore, it is ensured that the second trip of agents who did not arrive at their DCFC will not depart.

9.2 Induced demand

The induced demand on the traffic network is provided in terms of average time spent in queues, in particular, scenarios are compared based on the difference that agents perceive. In all investigated scenarios, 7% of all vehicles is assumed to be a BEV and will charge on their route. For

the total demand data, that would be 12,300 BEVs out of the total 176,000 agents. However, for simulation time purposes only the morning rush hours are considered in line with Chapter 8, hence the number of trips and agents is much smaller (20,400 agents for the base scenario). Note that in the base scenario, only a small percentage of the same group of BEVs charges at the DCFC on 3000 Telegraph Avenue. These EVs are considered as background traffic in the base scenario, e.g. similar to people visiting the Whole Foods Supermarket located on the same address, since Replica does not keep track of DCFC, or CS more generally, as possible trip purpose. Additionally, it was confirmed that percentage of EVs charging at DCFCs, in particular of the autumn 2021 data, was lower than the total share of BEVs as explained in Section 5.5.

Figure 9.1 provides a geographic representation of the difference in vehicle queue time between the scenario 1 and the base case. Queue time is interpreted as the additional average queue time for all vehicles on the presented links. A positive queue time obviously results in longer shorter travel time, which is undesirable and therefore depicted in red, links where agents experience negative queue times are depicted in green. Note that the reroute frequency is set to 2 minutes, due to which agents will reconsider their route choice and not wait in line to join the queue on the connecting link, which would have been the shortest path in an uncongested network where all travel times equal link free-flow time. Table 9.1 provides an overview of the number of number of agents that fully completed their trip, i.e. reaching the final destination not DCFC, and the average travel time for all scenarios where route choice revision happens every 2 minutes. The next section will shed a light on the effects of not considering the reroute option.

Table 9.1 Number of completed trips and the corresponding average travel time for all agents for each scenario with rerouting frequency set to 2 minutes.

Scenario	Completed trips	Charge trips	Average travel time
Base	20,400	0	279 s
Scenario 1	18,100	5,130	1,790 s
Scenario 2	17,400	4,860	1,830 s
Scenario 3	16,700	4,640	1,080 s

As can be seen in Figure 9.1, agents are likely to experience higher additional queuing time close to the DCFC locations, which have been provided in Figure 8.1 for scenario 1. Note that, the figures of the other scenarios will be provided in Section C.2 because a these show a very similar response of traffic queue time around DCFC locations.

Figure 9.1 Queue difference for all links in the traffic network of scenario 1 versus the base case without charging expressed as (average) queue time for all vehicles that traverse over that link. Agents reroute every 2 minutes.

9.2.1 Without route revision

Figure 9.2 provides a geographic representation of the difference in vehicle queue time between the scenario 1 and the base case. In this case, rerouting is not allowed. The result shows more network links are exhibit additional queuing time and that less links are used: agents avoid getting stuck in queues by diverting to residential, or smaller, streets. Similar to the results of scenario 1 where rerouting is considered, additional queuing time is observed around DCFC locations. Table 9.2 provides an overview of the number of total number of completed trips and the average travel time for all scenarios provided agents may not revise their route choice.

9.2.2 Effect of rerouting

In order to study the effect of allowing agents to revise their path choice, a visualisation of the queue difference between scenario 1 with and without rerouting is provided. This serves as an insight into the links that actually cause the additional travel time for agents, which has been analysed in Section 6.2. The red coloured links in the figure correspond to a higher queue time

Table 9.2 Number of completed trips and the corresponding average travel time for all agents for each scenario without rerouting.

Scenario	Completed trips	Charge trips	Average travel time
Base	20,400	0	278 s
Scenario 1	10,600	3,370	842 s
Scenario 2	7,800	2,000	942 s
Scenario 3	8,890	2,460	558 s

perceived by agents in the simulation where rerouting is allowed, in comparison to the simulation where agents may not revise their route choice. Consequently, green links portray a decrease in queue time and therefore a "better link travel time", in the simulation where rerouting is allowed. Figure 9.3 shows that areas around the DCFCs, e.g. close to the UC campus around University Avenue, became less congested.

Figure 9.2 Queue difference for all links in the traffic network of scenario 1 versus the base case without charging expressed as (average) queue time for all vehicles that traverse over that link. Agents do not revise their route.

Figure 9.3 Queue difference for all links in the traffic network of scenario 1 with rerouting versus the scenario 1 without rerouting expressed as (average) queue time for all vehicles that traverse over that link.

10

Conclusions

This chapter provides an interpretation of the results presented in Chapter 9. The first section concludes about the effect that different placement policies have on traffic, queue time in particular. The second section concludes about the effect that rerouting exhibits on the obtained results.

10.1 Evaluation of scenarios

Table 9.1 shows that average travel time in all scenarios with presence of BEVs which charge is higher. The charging time of 30 minutes and the share of BEVs that travel through the network explain that scenarios with BEVs show higher travel time and lower trip completion: queues build op when agents are waiting to get charged, this also affects agents with ICEVs who use the same links in their paths.

Travel times are equal to the average travel time for all completed individual trips, provided that agents selfishly minimise their travel time based on the observed traffic network conditions and through the use of the sp algorithm according to Section 7.3. The additional link travel time, or queue time, in all scenarios is relatively small. An additional 150 seconds, which is approximately equal to largest value from the simulation corresponds to one and a half full red light cycles, which are 90 seconds on average. Though, if this is the case on many consecutive links, this cumulative queuing time might have a major impact at overall travel times, even for agents that do not charge.

Simulation results of scenario 3, i.e. the clustered DCFC placement policy, where additional DCFCs are placed near the current existing DCFC on 3000 Telegraph Avenue, seems to yield the lowest travel times among all investigated scenarios. However, the number of completed trips is the lowest in this scenario: only 81.9% of all trips actually arrive, which means that the actual travel time likely to be much higher, as there is no data stored on travel time of agents who have not finished their trip yet. The placement policy in scenario 1, i.e. DCFC placement with large spatial

separation, yields the highest trip completion of 88.7%. Moreover, more vehicles have actually completed their charging trip in this scenario: 5.56% more than scenario 2, i.e. DCFC placement close to most trip origins, and 10.6% more than scenario 3.

Scenario 2 is regarded to as the worst placement policy among the investigated ones: less trips were completed, less vehicles charged and still the average travel time of agents in the second scenario is higher than of scenario 1. It is concluded that scenario 1 is the best placement policy, mainly because of the high trip completion and DCFC utilisation. Herewith, the sixth research sub-question has been answered.

10.2 Effect of rerouting

It can be seen in Figure 9.2 that single observation and route choice limits the use of many residential streets when comparing to the simulations where rerouting is allowed. Many residential streets leading to Ashby Avenue, which is the high capacity road that provides access to the DCFC on Telegraph for traffic heading eastbound and to the DCFCs on Seventh and Shellmound for traffic heading westbound. Ashby itself shows a couple of congested segments, the light red links, as well. The streets which are used in this scenario without rerouting show higher average vehicle queue time, this can be explained through the nature of single route choice alone: the route is chosen in the beginning of the simulation, as stated in Chapter 6, and hence based on less congested network links. Consequently, rerouting results in more widespread traffic across Berkeley, which results in higher VKT. Agents experience shorter a travel time when they revise their route choice and hence, there may be a smaller incentive to use higher capacity roads resulting in a trip of shorter distance rather than shortest travel time which might lead to trips of larger distance.

In the results section, focus is on the simulations with route revision. This is done because queues in the simulation without route revision cause many trips not to be completed due to agents getting stuck in queues as can be seen in the low trip completion provided in Table 9.2, in contrast to the trip completion of simulation with rerouting provided in Table 9.1. In conclusion, number of completed trips for simulations with route revision are more in the range of the base scenario and hence allow for more reliable comparison of additional travel, or queue, time.

10.3 Bottleneck identification

It can be seen in the previous figures that particular areas, especially close to the DCFC locations become more congested. The newly dark red links are bottlenecks of the traffic network that do

not allow for uninterrupted vehicular flow, as all vehicles traversing through the dark red links on average perceive a 2 minute travel time increase. For the best scenario, bottleneck forms in the Emeryville and Elmwood areas, in line with Table A.2. The congestion in Emeryville originates from vehicles charging at the DCFC on Shellmound Way. For Elmwood specifically, major congestion happens on the 3000 block on Telegraph Avenue block as well as the 2300 block on Ashby Avenue and is caused by the DCFC on Telegraph Avenue. Herewith, the seventh and last sub-question is answered. Furthermore, it can be seen that also the DCFC on University Avenue causes some congestion on the eastbound 1900 block of there.

10.4 The effect of induced demand on traffic

Concluding from the previous sections, vehicles experience the most highest queue time, or congestion, on the roads that provide access to the newly placed DCFCs. This holds true also for the simulation results of scenario 2 as can be seen in Figure C.3, queues formed close to the UC campus, and around the intersection of Dwigth and Shattuck, both in Southside. Queues close to campus explained by vehicles going to the DCFCs on University and Shattuck, whilst the queues around the hospital on the 2000 block of Dwigth Way are logically explained by the DCFC that is placed right there. Herewith, the main research question is answered.

11

Discussion

This chapter provides a discussion on the reliability of the findings of this study. Limitations in the methods used to obtain results will be provided in the following section and suggestions will be put forward to get rid of the listed limitations.

11.1 Dynamic charging behaviour

The time window of simulations is 6 hours in the morning rush hours for obtaining results, and the demand data of Replica allows for 24 hours. However, in order to model charging behaviour more realistically, the simulation time should be extended. As agents might for example use a public DCFC once every two days. Moreover, the use of DCFCs heavily depends on their distance travelled and on the battery capacity of the particular BEV.

Dynamic charging behaviour can be modelled through dynamic SOC. In the current simulation set-up, all BEVs charge at the start of their trip, this limitation can be resolved by modelling a dynamic SOC. With data from vehicle registering body such as California's Department of Motor Vehicles (DMV) [60], the share of BEVs and their specifics can be replicated accurately since there is data on vehicle brands, types and their battery capacity. This data allows for realistic representation of the BEV population. When an initial SOC is assumed at the beginning of each simulation according to a probability distribution, e.g. a uniform distribution between 20% and 80%, real-time charging demand can be modelled.

11.2 Limitations of the case study

Even though it might seem that relatively low penetration was used for case study of Berkeley, this share of BEVs is still much higher than the current. For the case study, all 7% of EVs were considered to be BEVs. Provided the total number of vehicles remains relatively stable, this entails

an approximate increase in BEVs of 60% compared to the current situation, which is approximately 4%, as can be reduced from Section A.3. To accommodate for this large increase of BEVs, an additional 3 DCFCs have been taken into consideration for placement. The ABM does allow for easy up-scaling of EV penetration, as the share of (B)EVs is simply an input to OD demand creation as explained in Section 8.1.

11.3 Charging preference

Some studies point out that a large share of refueling occurs along the commute route [85], which is demonstrated using case study in Northern California, or along other trips, e.g. trips that are linked to other shopping trips when shopping occurs slightly farther from home [57]. Hence, agents might combine the visit to the DCFC with doing quick groceries shopping, which makes sense because of the waiting time for a BEV to get charged. Additionally, peoples personal preference of DCFC locations, e.g. because of amenities such as restrooms or a nearby coffee place, are not taken into consideration in charging demand assignment.

11.3.1 Application of route choice learning

Research of 7,979 PEV owner's charging behaviour in California concludes that people who own a BEV and use public infrastructure only are more likely to be renters, apartment or condominium residents and have a lower likelihood of having access to workplace charging [64]. Reinforcement learning (RL), through the use of neural networks on historical data, such as data used in [64] might allow to predict weekly DCFC utilisation, provided inputs such as income, age, gender and housing type. Moreover, Replica is able provide trip-taker information such as building use, e.g. multi-family residential, and workplace location block group, which allows retracing the availability of workplace CSs. These parameters can be used to predict charging demand using Replica's data, possibly in combination with the EVI-Pro tool [58].

An example of route choice learning through route experience sharing is found in [86], agents individually determine the best route from their origin to their destination based on information from all agents. The authors do remark that actions are highly coupled, this non-cooperative learning is not a trivial task, since travel times are highly dependent on the route choice of other agents. However, this might experience sharing might potentially allow for estimating and translating DCFC preference, as mentioned in the previous section, into actual trips.

11.4 Data availability

As stated in Section 9.2, the OD demand data obtained from Replica does not identify (fast) charging as a trip purpose, nor does it distinguish between EVs and other vehicles, e.g. ICEVs. For future studies it would be useful not to rely on assumptions to get a clear insight in when agents decide to charge, as well as an understanding of the exact charging time. Currently, there is no information on the willingness to charge in terms of acceptable waiting time. Charging time is assumed to take 30 minutes for all vehicles, which is not the case logically. Information from companies that provide charging services may allow for the creation of a probability distribution for charging time. Then, agents in the simulation get assigned a charging time from the distribution. Note that this is not possible with the current set-up of accommodating for charging in the model. Currently, the DCFC access links are all given a constant traversing time, these could easily be changed to match the potential charge time distribution, but will then be remain constant throughout the simulation, since the `link_data` data-frame remains untouched during simulation.

11.4.1 Inter-city traffic

It would make sense to research locations along freeways as a charging policy as well, e.g. in the case study along the Interstate 580/80. However, since all trips starting or ending further than 500 m outside of the network are disregarded (Section 5.1), much of the traffic that simply travels through the area of study without stopping is not considered. Hence, researching a placement policy where DCFCs are placed close to the freeway does not make sense: it is not realistic that EVs part of inter-city traffic will redirect to get charged close to the freeway when this is not close to their route.

Arguments of the previous section are also used to explain why a DCFC placement policy along the main arterial roads, i.e. the roads which directly lead to the freeway, has not been studied: the OD demand data of the inter-city traffic logically does not include trips that use the freeway to leave the area of study, e.g. for people who commute from Berkeley to other cities.

11.4.2 Vehicles leaving the OSM network

As explained before, demand data is assigned to the closest node in the OSM network and trips with origins or destinations outside of the network are disregarded. A method that might allow for the inclusion of other trips than only inter-city traffic, sink nodes may be created near freeway entrance points to assign destinations of trips leaving, or origins of trips arriving in, the network model. Then, the challenge becomes assigning trip destinations to the right sinks in the network, i.e. to the location where the agents actually leave the network model. Here is an example to

illustrate this challenge: a person who lives in Berkeley and works in Walnut Creek, a city located to the east of Berkeley, will exit the Berkeley area on the south to merge onto California highway 24 to get to work, and take the tunnel under the Berkeley Hills to get there, as that is the shortest path of this OD pair. However, the geographically closest network node to this destination might be a intersection high in the Berkeley Hills connecting low-capacity roads, which would lead to an unrealistic trip through the network, as the agent is routed into the small roads Berkeley Hills instead of to the freeway, what the agent would do in the real world.

12

Future extensions

This final chapter presents future extensions for this research. The two sections provide a connection between the literature of respective research topics and potential opportunities for the use of modelling methodology and results from this study.

12.1 Emissions shifting

It has been established in the past that faster highway route choice are not always the best from both an environmental and energy consumption perspective. Significant improvements to energy and air quality can be achieved when vehicles utilize a slower arterial route even though their travel time is longer [87]. Additionally, traffic congestion and traffic volume contributed much more to air pollution than the impact of fluctuating terrain [88]. The ABM and the methodology for data presentation and handling used in this study can be used to model relocation of emissions resulting from different route choices and study, and potentially resolve, resulting bottlenecks.

12.2 Managing bottleneck congestion

In the literature, various solutions have been proposed to reduce bottleneck congestion [89], examples of which are price on the use of the bottleneck roads through tolling [90, 91] or rewarding vehicles that enter bottleneck areas outside of rush hours through the use of incentive based traffic demand management [92]. [89] puts forward an incentive-based traffic demand management policy to alleviate traffic congestion on a road stretch that creates a bottleneck for the commuters. Provided the increase in BEV adoption in the future and the simulation results, which show different locations of queue forming, placement of DCFCs may be used to steer vehicles away from roads prone to bottleneck forming in rush hours, i.e. with the goal to improve social cost in terms of travel time for all vehicles. The methodology described in Chapter 5 can easily be used to model trips for any share of EVs.

References

1. Muratori, M. *et al.* The rise of electric vehicles—2020 status and future expectations. *Progress in Energy* **3,** 022002. https://dx.doi.org/10.1088/2516-1083/abe0ad (Mar. 2021).

2. IEA. *Electric Vehicles* 2022. https://www.iea.org/reports/electric-vehicles.

3. *Paris Declaration on Electro-Mobility and Climate Change & Call to Action* 2015. https://newsroom.unfccc.int/news/the-paris-declaration-on-electro-mobility-and-climate-change-and-call-to-action.

4. Neaimeh, M. *et al.* Analysing the usage and evidencing the importance of fast chargers for the adoption of battery electric vehicles. *Energy Policy* **108,** 474–486. ISSN: 0301-4215. https://www.sciencedirect.com/science/article/pii/S0301421517303877 (2017).

5. Funke, S. Á., Sprei, F., Gnann, T. & Plötz, P. How much charging infrastructure do electric vehicles need? A review of the evidence and international comparison. *Transportation Research Part D: Transport and Environment* **77,** 224–242. ISSN: 1361-9209. https://www.sciencedirect.com/science/article/pii/S136192091930896X (2019).

6. Levinson, R. S. & West, T. H. Impact of public electric vehicle charging infrastructure. *Transportation Research Part D: Transport and Environment* **64.** The contribution of electric vehicles to environmental challenges in transport. WCTRS conference in summer, 158–177. ISSN: 1361-9209. https://www.sciencedirect.com/science/article/pii/S136192091630757X (2018).

7. *Site information for electric vehicle Direct Current Fast Chargers* 2022. https://www.pge.com/en_US/about-pge/environment/what-we-are-doing/electric-program-investment-charge/direct-current-electric-vehicle-fast-chargers.page.

8. Li, S., Tong, L., Xing, J. & Zhou, Y. The market for electric vehicles: indirect network effects and policy design. *Journal of the Association of Environmental and Resource Economists* **4,** 89–133 (2017).

9. Chakraborty, D., Bunch, D. S., Brownstone, D., Xu, B. & Tal, G. Plug-in electric vehicle diffusion in California: Role of exposure to new technology at home and work. *Transportation Research Part A: Policy and Practice* **156,** 133–151 (2022).

10. Hardman, S., Chandan, A., Tal, G. & Turrentine, T. The effectiveness of financial purchase incentives for battery electric vehicles – A review of the evidence. *Renewable and Sustainable Energy Reviews* **80,** 1100–1111. ISSN: 1364-0321. https://www.sciencedirect.com/science/article/pii/S1364032117309012 (2017).

11. *State of California. Executive Order N-79-20* 2020. https://www.gov.ca.gov/wp-content/uploads/2020/09/9.23.20-EO-N-79-20-Climate.pdf?emrc=9f8f26.

12. Broadbent, G. H., Drozdzewski, D. & Metternicht, G. Electric vehicle adoption: An analysis of best practice and pitfalls for policy making from experiences of Europe and the US. *Geography Compass* **12.** ISSN: 17498198 (Feb. 2018).

13. Narassimhan, E. & Johnson, C. The role of demand-side incentives and charging infrastructure on plug-in electric vehicle adoption: analysis of US States. *Environmental Research Letters* **13,** 074032. https://dx.doi.org/10.1088/1748-9326/aad0f8 (July 2018).

14. Neubauer, J. & Wood, E. The impact of range anxiety and home, workplace, and public charging infrastructure on simulated battery electric vehicle lifetime utility. *Journal of Power Sources* **257,** 12–20. ISSN: 0378-7753. https://www.sciencedirect.com/science/article/pii/S0378775314000998 (2014).

15. Moloughney, T. *The Best Home EV Charger Buying Guide For 2020* 2020. https://insideevs.com/features/341500/the-ultimate-buyers-guide-to-home-ev-chargers-plus-top-5-picks/.

16. *How Many Watts Can An Outlet Handle? (110V,120V,220V + 15,20,30A Breakers), HVAC Systems* 2022. https://learnmetrics.com/how-many-watts-can-an-outlet-handle/.

17. ENGIE. *Alles wat je moet weten over een 1-fase laadpaal* 2022. https://www.evstore.nl/kennisbank/1-fase-laadpaal/.

18. *Electric Vehicle Charging Speeds, Rural EV Toolkit* 2022. https://www.transportation.gov/rural/ev/toolkit/ev-basics/charging-speeds.

19. Ahmed, S. I., Salehfar, H. & Selvaraj, D. F. *Impact of Electric Vehicle Charging on the Performance of Distribution Grid* in *2021 IEEE 12th International Symposium on Power Electronics for Distributed Generation Systems (PEDG)* (2021), 1–8.

20. Brenna, M., Foiadelli, F., Leone, C. & Longo, M. Electric Vehicles Charging Technology Review and Optimal Size Estimation. *Journal of Electrical Engineering & Technology volume* **15,** 2539–2552 (2020).

21. X., Z., B., M. & P., M. Grid impact analysis of heavy-duty electric vehicle charging stations. *IEEE Power Energy Society Innovative Smart Grid Technologies Confer- ence (ISGT)* **9,** 1–5 (2020).

22. Rizvi, S. A. A. *et al. Electric Vehicles and their Impacts on Integration into Power Grid: A Review* in *2018 2nd IEEE Conference on Energy Internet and Energy System Integration (EI2)* (2018), 1–6.

23. *Time of use* 2022. https://svcleanenergy.org/time-of-use/.

24. Dincer, I. & Erdemir, D. in *Heat Storage Systems for Buildings* (eds Dincer, I. & Erdemir, D.) 37–90 (Elsevier, 2021). ISBN: 978-0-12-823572-0. https://www.sciencedirect.com/science/article/pii/B9780128235720000102.

25. Hudson, T. *Power Factor Correction (PFC)* 2022. https://www.monolithicpower.com/en/power-factor-correction.

26. Shahnia, F., Ghosh, A., Ledwich, G. & Zare, F. *Voltage unbalance sensitivity analysis of plug-in electric vehicles in distribution networks* in *AUPEC 2011* (2011), 1–6.

27. Brenna, M., Foiadelli, F., Leone, C. & Longo, M. Electric vehicles charging technology review and optimal size estimation. *Journal of Electrical Engineering & Technology* **15,** 2539–2552 (2020).

28. Meyer, J., Hähle, S., Schegner, P. & Wald, C. *Impact of electrical car charging on unbalance in public low voltage grids* in *11th International Conference on Electrical Power Quality and Utilisation* (2011), 1–6.

29. Meyer, J., Hähle, S., Schegner, P. & Wald, C. *Power factor correction* in *IEE Writing Matters* (2006), 22–24.

30. Rini Ann Jerin, A. *et al.* in *Hybrid-Renewable Energy Systems in Microgrids* (eds Fathima, A. H. *et al.*) 195–202 (Woodhead Publishing, 2018). ISBN: 978-0-08-102493-5. https://www.sciencedirect.com/science/article/pii/B9780081024935000108.

31. Nute, R. *Transients in Secondary Circuits* Aug. 2016. https://incompliancemag.com/article/transients-in-secondary-circuits/.

32. Panossian, N. *et al.* Challenges and Opportunities of Integrating Electric Vehicles in Electricity Distribution Systems. *Current Sustainable/Renewable Energy Reports* **9,** 29–40 (2022).

33. Ahmad, F., Iqbal, A., Ashraf, I., Marzband, M. & khan, I. Optimal location of electric vehicle charging station and its impact on distribution network: A review. *Energy Reports* **8,** 2314–2333. ISSN: 2352-4847. https://www.sciencedirect.com/science/article/pii/S2352484722001809 (2022).

34. Lam, A. Y., Leung, Y.-W. & Chu, X. Electric vehicle charging station placement: Formulation, complexity, and solutions. *IEEE Transactions on Smart Grid* **5,** 2846–2856 (2014).

35. Tushar, W., Saad, W., Poor, H. V. & Smith, D. B. Economics of electric vehicle charging: A game theoretic approach. *IEEE Transactions on Smart Grid* **3,** 1767–1778 (2012).

36. Pashajavid, E. & Aliakbar Golkar, M. Optimal placement and sizing of plug in electric vehicles charging stations within distribution networks with high penetration of photovoltaic panels. *Journal of Renewable and Sustainable Energy* **5** (Sept. 2013).

37. Chen, L., Xu, C., Song, H. & Jermsittiparsert, K. Optimal sizing and sitting of EVCS in the distribution system using metaheuristics: A case study. *Energy Reports* **7,** 208–217. ISSN: 2352-4847. https://www.sciencedirect.com/science/article/pii/S2352484720317364 (2021).

38. Zeb, M. Z. *et al.* Optimal Placement of Electric Vehicle Charging Stations in the Active Distribution Network. *IEEE Access* **8,** 68124–68134 (2020).

39. Luo, C., Huang, Y.-F. & Gupta, V. Placement of EV Charging Stations—Balancing Benefits Among Multiple Entities. *IEEE Transactions on Smart Grid* **8,** 759–768 (2017).

40. Shukla, A., Verma, K. & Kumar, R. Multi-objective synergistic planning of EV fast-charging stations in the distribution system coupled with the transportation network. *IET generation, transmission & distribution* **13.** ISSN: 1751-8687 (Aug. 2019).

41. Kumar, P. in *Logistics, supply chain and financial predictive analytics* 195–209 (Springer, 2019).

42. *Nieuwe knelpunten op het elektriciteitsnet in Noord-Holland* 2021. https://www.liander.nl/nieuws/2021/09/16/nieuwe-knelpunten-op-het-elektriciteitsnet-noord-holland.

43. Boeing, G. *User reference* 2016. https://osmnx.readthedocs.io/en/stable/osmnx.html?highlight=intersection_consolidation#osmnx.stats.intersection_count.

44. Replica. *About Replica* 2022. https://replicahq.com/about/.

45. Zhao, B., Kumar, K., Casey, G. & Soga, K. *Agent-based model (ABM) for city-scale traffic simulation: A case study on San Francisco* in *International Conference on Smart Infrastructure and Construction 2019 (ICSIC) Driving data-informed decision-making* (2019), 203–212.

46. Zhao, B. & Wong, S. D. Developing transportation response strategies for wildfire evacuations via an empirically supported traffic simulation of Berkeley, California. *Transportation research record* **2675,** 557–582 (2021).

47. Dijkstra, E. *A note on two problems in connexion with graphs. Numeriske Mathematik, 1, 269–271* 1959.

48. Rudjanakanoknad, J. Capacity Change Mechanism of a Diverge Bottleneck. *Transportation Research Record* **2278,** 21–30. eprint: https://doi.org/10.3141/2278-03. https://doi.org/10.3141/2278-03 (2012).

49. *Node* 2022. https://wiki.openstreetmap.org/wiki/Node.

50. Behrisch, M., Bieker, L., Erdmann, J. & Krajzewicz, D. *SUMO–simulation of urban mobility: an overview* in *Proceedings of SIMUL 2011, The Third International Conference on Advances in System Simulation* (2011).

51. Eason, T., Chuang, W.-C., Sundstrom, S. & Cabezas, H. An information theory-based approach to assessing spatial patterns in complex systems. *Entropy* **21,** 182 (2019).

52. Veness, C. *Calculate Distance, Bearing and More between Latitude/Longitude Points* 2019. https://www.movable-type.co.uk/scripts/latlong.html.

53. Maria, E., Budiman, E., Haviluddin & Taruk, M. Measure distance locating nearest public facilities using Haversine and Euclidean Methods. *Journal of Physics: Conference Series* **1450,** 012080. https://dx.doi.org/10.1088/1742-6596/1450/1/012080 (Feb. 2020).

54. IEA. *Electric Vehicles* 2022. https://electricvehicles.bchydro.com/how-use-our-fast-chargers/how-long-can-i-charge-fast-charging-station.

55. Specialist), C. (C. O. private communication. 2023.

56. *Site information for electric vehicle Direct Current Fast Chargers* 2016. https://www.pge.com/en_US/about-pge/environment/what-we-are-doing/electric-program-investment-charge/direct-current-electric-vehicle-fast-chargers.page.

57. Nicholas, M. A. Driving demand: What can gasoline refueling patterns tell us about planning an alternative fuel network? *Journal of Transport Geography* **18,** 738–749 (2010).

58. AFDC. *Electric Vehicle Infrastructure Projection Tool (EVI-Pro) Lite* 2022. https://afdc.energy.gov/evi-pro-lite/load-profile/results?utf8=%E2%9C%93&load_profile%5C%5Bstate%5C%5D=CA&load_profile%5C%5Burban_area%5C%5D=San+Francisco+-+Oakland&load_profile%5C%5Bstate_name%5C%5D=California&load_profile%5C%5Bfleet_size%5C%5D=1000&load_profile%5C%5Bmean_dvmt%5C%5D=35&load_profile%5C%5Bclass_dist%5C%5D=Sedan&load_profile%5C%5Bwork_power_dist%5C%5D=MostL2&load_profile%5C%5Bhome_access_dist%5C%5D=HA100&load_profile%5C%5Bhome_power_dist%5C%5D=Equal&load_profile%5C%5Bpref_dist%5C%5D=Home100&commit=Calculate#.

59. Ucer, E. *et al.* Modeling and analysis of a fast charging station and evaluation of service quality for electric vehicles. *IEEE Transactions on Transportation Electrification* **5,** 215–225 (2019).

60. *Light-Duty Vehicle Population in California, 2021* 2022. https://www.energy.ca.gov/zevstats.

61. *Fall 2021 Weather History in Berkeley California, United States* 2022. https://weatherspark.com/s/491/2/Average-Fall-Weather-in-Berkeley-California-United-States.

62. *Charging at Home* https://www.energy.gov/energysaver/articles/ev-charging-home.

63. O'Connor, P., Barnes, N. & Urquhart, K. *The Expanding EV Market. Observations in a year of growth* Feb. 2022. https://pluginamerica.org/wp-content/uploads/2022/03/2022-PIA-Survey-Report.pdf.

64. Lee, J. H., Chakraborty, D., Hardman, S. J. & Tal, G. Exploring electric vehicle charging patterns: Mixed usage of charging infrastructure. *Transportation Research Part D: Transport and Environment* **79,** 102249. ISSN: 1361-9209. https://www.sciencedirect.com/science/article/pii/S136192091831099X (2020).

65. Kiang, Y.-H. in *Fuel Property Estimation and Combustion Process Characterization* (ed Kiang, Y.-H.) 11–39 (Academic Press, 2018). ISBN: 978-0-12-813473-3. https://www.sciencedirect.com/science/article/pii/B9780128134733000027.

66. Kim, S. & Kim, H. A new metric of absolute percentage error for intermittent demand forecasts. *International Journal of Forecasting* **32,** 669–679. ISSN: 0169-2070. https://www.sciencedirect.com/science/article/pii/S0169207016000121 (2016).

67. Szeto, W. & Lo, H. K. Dynamic traffic assignment: properties and extensions. *Transportmetrica* **2,** 31–52 (2006).

68. Kuznets, S. Random events and cyclical oscillations. *Journal of the American Statistical Association* **24,** 258–275 (1929).

69. Alvarez-Ramirez, J., Rodriguez, E. & Carlos Echeverría, J. Detrending fluctuation analysis based on moving average filtering. *Physica A: Statistical Mechanics and its Applications* **354,** 199–219. ISSN: 0378-4371. https://www.sciencedirect.com/science/article/pii/S0378437105001524 (2005).

70. Manual, T. A. Bureau of Public Roads, US Dept. *Commer., Washington, DC, USA* (1964).

71. Brederode, L., Bliemer, M. & Wismans, L. *STAQ: Static Traffic Assignment with Queing* in *ETC 2010: European Transport Conference, Glasgow, UK, 11-13 October 2010* (2010).

72. Maerivoet, S. & De Moor, B. Transportation Planning and Traffic Flow Models (July 2005).

73. Iryo, T. Properties of dynamic user equilibrium solution: existence, uniqueness, stability, and robust solution methodology. *Transportmetrica B: Transport Dynamics* **1,** 52–67. eprint: https://doi.org/10.1080/21680566.2013.779793. https://doi.org/10.1080/21680566.2013.779793 (2013).

74. Nagurney, A. *Network economics: A variational inequality approach* (Kluwer Academic Publishers. Norwell, Massachusetts, USA., 1993).

75. Beckmann, M., McGuire, C. B. & Winsten, C. B. *Studies in the Economics of Transportation* tech. rep. (1956).

76. Krylatov, A., Zakharov, V. & Tuovinen, T. in *Optimization Models and Methods for Equilibrium Traffic Assignment* 17–43 (Springer International Publishing, Cham, 2020). ISBN: 978-3-030-34102-2. https://doi.org/10.1007/978-3-030-34102-2_2.

77. Wardrop, J. G. Road paper. some theoretical aspects of road traffic research. *Proceedings of the institution of civil engineers* **1,** 325–362 (1952).

78. Nie, X. & Zhang, H. M. A comparative study of some macroscopic link models used in dynamic traffic assignment. *Networks and Spatial Economics* **5,** 89–115 (2005).

79. Burov, M., Kizilkale, C., Kurzhanskiy, A. & Arcak, M. *Detecting braess routes: An algorithm accounting for queuing delays with an extended graph* in *2021 IEEE International Intelligent Transportation Systems Conference (ITSC)* (2021), 2125–2130.

80. Jin, W.-L. Point queue models: A unified approach. *Transportation Research Part B: Methodological* **77,** 1–16. ISSN: 0191-2615. https://www.sciencedirect.com/science/article/pii/S0191261515000430 (2015).

81. Szeto, W. Y. *Dynamic traffic assignment: formulations, properties, and extensions* (Hong Kong University of Science and Technology (Hong Kong), 2003).

82. Ge, Y. & Zhou, X. An alternative definition of dynamic user optimum on signalised road networks. *Journal of Advanced Transportation* **46,** 236–253 (2012).

83. Ge, Y., Sun, B., Zhang, H., Szeto, W. & Zhou, X. A comparison of dynamic user optimal states with zero, fixed and variable tolerances. *Networks and Spatial Economics* **15,** 583–598 (2015).

84. Tal, G. *et al.* Advanced Plug-in Electric Vehicle Travel and Charging Behavior Final Report. *California Air Resources Board Contract,* 40–46 (2020).

85. Kitamura, R. & Sperling, D. Refueling behavior of automobile drivers. *Transportation Research Part A: General* **21,** 235–245 (1987).

86. Klügl, F. & Bazzan, A. L. C. Accelerating route choice learning with experience sharing in a commuting scenario: An agent-based approach. *AI Communications* **34,** 105–119 (2021).

87. Ahn, K. & Rakha, H. The effects of route choice decisions on vehicle energy consumption and emissions. *Transportation Research Part D: Transport and Environment* **13,** 151–167. ISSN: 1361-9209. https://www.sciencedirect.com/science/article/pii/S1361920908000047 (2008).

88. Huboyo, H. S., Handayani, W. & Samadikun, B. P. Potential air pollutant emission from private vehicles based on vehicle route. *IOP Conference Series: Earth and Environmental Science* **70,** 012013. https://dx.doi.org/10.1088/1755-1315/70/1/012013 (June 2017).

89. Cenedese, C., Stokkink, P., Geroliminis, N. & Lygeros, J. Incentive-based electric vehicle charging for managing bottleneck congestion. *European Journal of Control* **68.** 2022 European Control Conference Special Issue, 100697. ISSN: 0947-3580. https://www.sciencedirect.com/science/article/pii/S0947358022000905 (2022).

90. Van den Berg, V. & Verhoef, E. T. Congestion tolling in the bottleneck model with heterogeneous values of time. *Transportation Research Part B: Methodological* **45,** 60–78 (2011).

91. Lindsey, C. R., Van den Berg, V. A. & Verhoef, E. T. Step tolling with bottleneck queuing congestion. *Journal of Urban Economics* **72,** 46–59 (2012).

92. Rye, T. & Ison, S. *The implementation and effectiveness of transport demand management measures: An international perspective* (Routledge, 2016).

93. *Busbar* Sept. 2022. https://en.wikipedia.org/wiki/Busbar.

94. *Distribution feeder definition* 2022. https://www.lawinsider.com/dictionary/distribution-feeder.

95. Vertiv. *Three-Phase Power: What It Is and the Benefits It Brings* 2022. https://www.vertiv.com/en-emea/about/news-and-insights/articles/educational-articles/three-phase-power-what-it-is-and-the-benefits-it-brings/.

APPENDICES

Appendix A

Data

A.1 Electricity distribution

Buses or bus bars allow for high current power distribution and are used to connect high voltage equipment at substations [93]. The generation source delivers electricity to substations from which a distribution feeder emerges that supplies customers [94], which exists of a three-phase set of conductors, i.e. three power lines that each supply alternating current, where each sinusoidal wave separated by one-third of the total wavelength, such that there is no point at which no power is being delivered to the distribution network [95].

A.2 OSM data

As mentioned in Section 5.2 and Section 5.4, both Figure 5.1 and Figure 5.3 are based on a real intersection in Berkeley, California, but is not scaled to true sizes. The opposing lanes of University Avenue in the OSM network are separately stored, they geographically appear as two unidirectional, separate roads: the top lane is unidirectional from east to west, i.e. from node 3 to 1, and the bottom lane is unidirectional from west to east, i.e. from node 2 to 4. Table A.1 displays the corresponding OSM ids and the geographical location, in terms of latitude, longitude and location of the intersection, of the nodes depicted in both graphs of Figure 5.3. Note that the network used in simulations may be simplified, e.g. University Avenue may be merged into one edge, removing redundant nodes whilst keeping the network connected.

Table A.1 Corresponding location information of Figure 5.3

Node	OSM id	Latitude	Longitude	Junction location OSM
1	53093985	37.8697564	-122.2875195	University/Bonar North
2	240448886	37.869652	-122.287496	University/Bonar South
3	53047340	37.8701714	-122.2842857	University/Acton North
4	240448888	37.8700588	-122.284267	University/Acton South
5	53093987	37.8687377	-122.2873227	Bonar/Addison

In the example used in Figure 5.3, the OSM node id `240448886` corresponds to the southern junction of University Avenue and Bonar Street, i.e. node 2 in Figure 5.3b. Note that these are the original OSM node IDs. After network consolidation, the nodes might be merged into new ones losing their original ID. Hence, for traceability purposes, the original, unedited OSM network data is used in this example. The OSM network, with the currently operational DCFC on 3000 Telegraph Avenue is provided in Figure A.1.

Figure A.1 OSM graph of Figure 3.1, with the existing DCFCs depicted with the red location pin.

A.3 OD demand data

The zip codes of the home locations of the considered trips in the OD data have been listed in Table A.2, all in Alameda County, California.

Table A.2 Zip codes of OD data.

Zip code	Neighbourhood	City
94608	Emeryville	Berkeley
94609	Temescal	Oakland
94618	Rockridge	Oakland
94702	West Berkeley	Berkeley
94703	South Berkeley	Berkeley
94704	Southside	Berkeley
94705	Elmwood	Berkeley
94706	Albany	Berkeley
94707	Thousand Oaks	Berkeley
94708	Berkeley Hills	Berkeley
94709	Northside	Berkeley
94710	West Berkeley	Berkeley
94720	Southside	Berkeley

In the considered zip codes, 6.86 percent of all vehicles were EVs in 2021: as there is a total of 7,762 EVs, of which there are 4,793 BEV and 2,969 PHEVs out of a total of 113,966 vehicles [60].

A.4 Charging demand

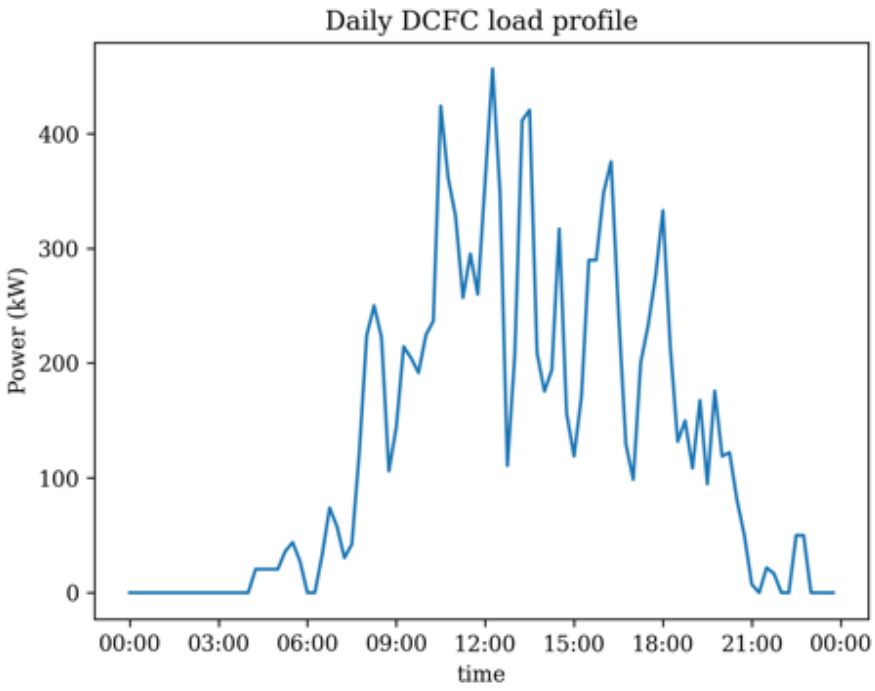

Figure A.2 Estimated DCFC hourly load profile for the Berkeley area obtained from the Alternative Fuels Data Center [58].

A.5 Pre-calibration ABM performance

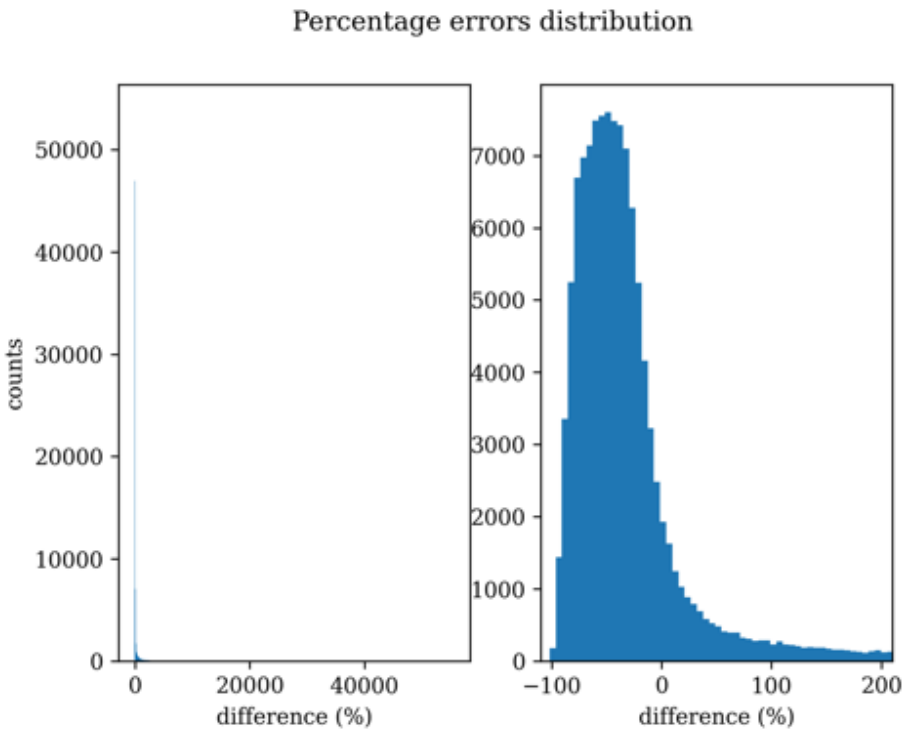

Figure A.3 Distribution of the arrival time percentage error for data of autumn 2021. The plot on the left displays the distribution of all trips and the plot on the right provides a zoomed view of that same distribution.

Appendix B

Code additions

B.1 Finding the closest DCFC

```
1  def cs_distances(start_node, end_node, cs_nodes, g=None):
2      sp_dist = []
3      for station in range(len(cs_nodes)):
4          sp = g.dijkstra(start_node, cs_nodes[station])
5          travel_time_from_origin_to_cs = sp.distance(cs_nodes[station])
6          sp.clear()
7          sp = g.dijkstra(cs_nodes[station], end_node)
8          travel_time_from_cs_to_destin = sp.distance(end_node)
9          sp.clear()
10         total_travel_time_with_charge = travel_time_from_origin_to_cs
               + travel_time_from_cs_to_destin
11         sp_dist.append(total_travel_time_with_charge)
12     index_closest = pd.Series(sp_dist).idxmin()
13     closest_cs = cs_nodes[index_closest]
14     return closest_cs
```

B.2 Moving average link capacity

Within the `queue_model.py`, a dictionary element is added to the Link class (which stores all link information for all iterations) called `cap_list`, it stores the leftover, or available, capacity for the current link. Then, the last 60 elements of the `cap_list` are extracted and divided by 60 to get the average available capacity at the current time step.

```
class Link:
    def __init__(self, link_id, lanes, length, fft, capacity, ltype,
        start_nid, end_nid, geometry, simulation=None):
        ### input
        ...
        self.cap_list = []
        self.cap_average = 0

    ...
    def run_link_model(self, t_now):
        self.st_c = self.store_cap - np.sum([self.simulation.
            all_agents[agent_id].veh_len for agent_id in self.run_veh+
            self.queue_veh])
        self.in_c, self.ou_c = self.capacity/3600, self.capacity/3600
        self.cap_list.append(self.st_c)
        self.cap_list = self.cap_list[-60:]
        self.cap_average = np.sum(self.cap_list) / len(self.cap_list)
```

Appendix C

Figures

C.1 Placement policies

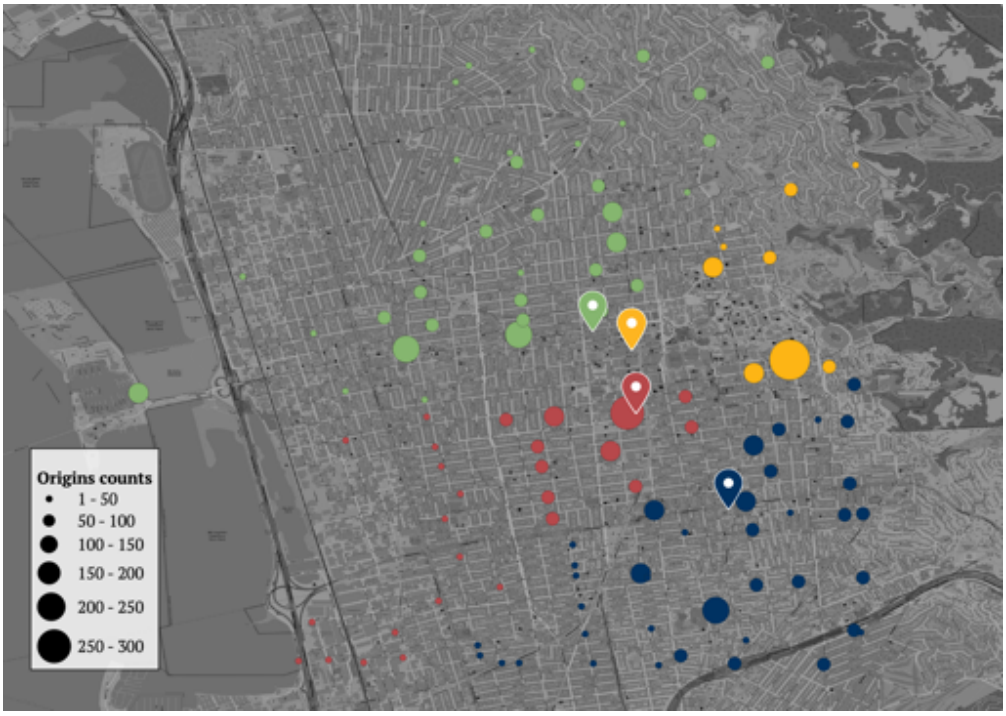

Figure C.1 Geographical representation of origins and their counts for all EV trips in scenario 2 going to the geographically closest DCFC in Berkeley, among the ones listed in Table 8.2. The colours depicting each DCFC in accordance with the order of Table 8.2 read blue, yellow, green and red.

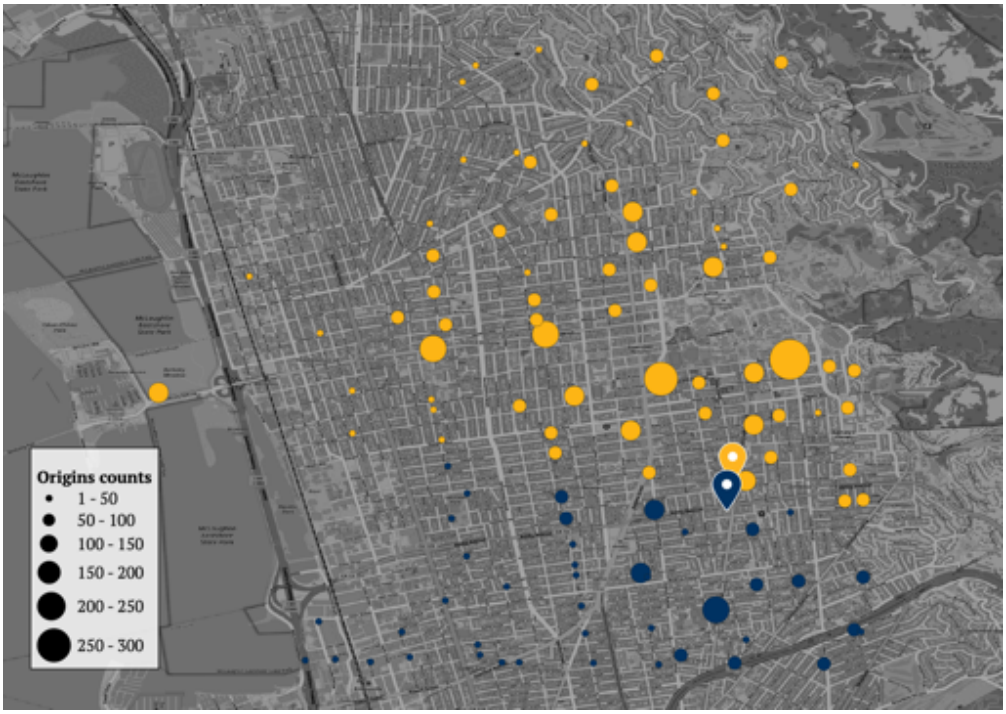

Figure C.2 Geographical representation of origins and their counts for all EV trips in scenario 2 going to the geographically closest DCFC in Berkeley, among the ones listed in Table 8.3. The colours depicting each DCFC in accordance with the order of Table 8.3 read blue and yellow.

C.2 Effect of placement on queues results

Figure C.3 Queue difference for all links in the traffic network of scenario 2 versus the base case without charging expressed as (average) queue time for all vehicles that traverse over that link.

Figure C.4 Queue difference for all links in the traffic network of scenario 3 versus the base case without charging expressed as (average) queue time for all vehicles that traverse over that link.